NAVAL POSTGRADUATE SCHOOL

MONTEREY, CALIFORNIA

THESIS

METAMATERIAL ABSORBERS FOR MICROWAVE DETECTION

by

Michael T. McMahan

June 2015

Thesis Advisor: Dragoslav Grbovic
Co-Advisor: Richard C. Olsen

Approved for public release; distribution is unlimited

THIS PAGE INTENTIONALLY LEFT BLANK

REPORT DOCUMENTATION PAGE

Form Approved OMB No. 0704–0188

1. AGENCY USE ONLY *(Leave blank)*	**2. REPORT DATE** June 2015	**3. REPORT TYPE AND DATES COVERED** Master's Thesis

4. TITLE AND SUBTITLE
METAMATERIAL ABSORBERS FOR MICROWAVE DETECTION

5. FUNDING NUMBERS

6. AUTHOR(S) Michael T. McMahan

7. PERFORMING ORGANIZATION NAME(S) AND ADDRESS(ES)
Naval Postgraduate School
Monterey, CA 93943-5000

8. PERFORMING ORGANIZATION REPORT NUMBER

9. SPONSORING /MONITORING AGENCY NAME(S) AND ADDRESS(ES)
N/A

10. SPONSORING/MONITORING AGENCY REPORT NUMBER

11. SUPPLEMENTARY NOTES The views expressed in this thesis are those of the author and do not reflect the official policy or position of the Department of Defense or the U.S. Government. IRB Protocol number ____N/A____.

12a. DISTRIBUTION / AVAILABILITY STATEMENT
Approved for public release; distribution is unlimited

12b. DISTRIBUTION CODE

13. ABSTRACT (maximum 200 words)

The development of high-power microwave weapons and dependence on electronics in modern weapon systems presents a high-power microwave weapons threat in future military conflicts. This study experimentally determines the absorption characteristics of simple metamaterial devices to potentially be used as protection and identification mechanisms, constructed through standard printed circuit board manufacturing processes, in the microwave region. Experimental results and analysis techniques are presented confirming absorption peaks in the anticipated microwave frequency range. The experimental results are compared to a finite-element model of these metamaterials confirming the ability to accurately model and predict absorption characteristics of similar metamaterial structures. Utilization of the absorption characteristics of these types of metamaterial structures to develop a microwave detector and/or equipment shielding is discussed. Several applications for such type of a detector are presented.

14. SUBJECT TERMS
metamaterials, metamaterial absorbers, metamaterial detectors

15. NUMBER OF PAGES
65

16. PRICE CODE

17. SECURITY CLASSIFICATION OF REPORT	**18. SECURITY CLASSIFICATION OF THIS PAGE**	**19. SECURITY CLASSIFICATION OF ABSTRACT**	**20. LIMITATION OF ABSTRACT**
Unclassified	Unclassified	Unclassified	UU

NSN 7540–01-280-5500

Standard Form 298 (Rev. 2–89)
Prescribed by ANSI Std. 239–18

THIS PAGE INTENTIONALLY LEFT BLANK

Approved for public release; distribution is unlimited

METAMATERIAL ABSORBERS FOR MICROWAVE DETECTION

Michael T. McMahan
Lieutenant Colonel, United States Marine Corps
B.S., San Jose State University, 1997

Submitted in partial fulfillment of the
requirements for the degree of

MASTER OF SCIENCE IN SPACE SYSTEMS OPERATIONS

from the

NAVAL POSTGRADUATE SCHOOL
June 2015

Author: Michael T. McMahan

Approved by: Dragoslav Grbovic
Thesis Advisor

Richard C. Olsen
Co-Advisor

Rudolf Panholzer
Chair, Space Systems Academic Group

THIS PAGE INTENTIONALLY LEFT BLANK

ABSTRACT

The development of high-power microwave weapons and dependence on electronics in modern weapon systems presents a high-power microwave weapons threat in future military conflicts. This study experimentally determines the absorption characteristics of simple metamaterial devices to potentially be used as protection and identification mechanisms, constructed through standard printed circuit board manufacturing processes, in the microwave region. Experimental results and analysis techniques are presented confirming absorption peaks in the anticipated microwave frequency range. The experimental results are compared to a finite-element model of these metamaterials confirming the ability to accurately model and predict absorption characteristics of similar metamaterial structures. Utilization of the absorption characteristics of these types of metamaterial structures to develop a microwave detector and/or equipment shielding is discussed. Several applications for such type of a detector are presented.

THIS PAGE INTENTIONALLY LEFT BLANK

TABLE OF CONTENTS

I. INTRODUCTION....1

II. HIGH POWER MICROWAVE WEAPONS OVERVIEW....3

III. HPM WEAPONS APPLICABILITY IN SPACE....9
- A. HPM WEAPONS AS ASATS....11

IV. METAMATERIALS....13

V. EXPERIMENTAL DATA COLLECTION AND ANALYSIS....17
- A. METAMATERIAL STRUCTURES DESCRIPTION....17
- B. DATA COLLECTION....18
- C. DATA ANALYSIS....20

VI. MODELING....33

VII. CONCLUSIONS....37
- A. SUMMARY OF RESULTS....37
- B. SENSOR APPLICABILITY....39
- C. SPACE APPLICABILITY....41
- D. FUTURE WORK....42

LIST OF REFERENCES....45

INITIAL DISTRIBUTION LIST....51

THIS PAGE INTENTIONALLY LEFT BLANK

LIST OF FIGURES

Figure 1. HPM susceptibility of integrated circuit technologies due to feature size, from [3]. 1

Figure 2. (a) In conventional materials ε and μ quantify how electrons respond to an electric field; in metamaterials, ε_{eff} and μ_{eff} are derived from the patterned elements which may contain many atoms. (b) An early example of a metamaterial with a resonant magnetic response. Split rings are etched onto a circuit board, from [20]. 14

Figure 3. (a) Plasmons flow along the boundary between a metal and a dielectric. Light incident to the grove in a metal generates plasmons that propagate along the metal surface (boundary between metal and air), from [37]. (b) Surface plasmons propagate along the metal/dielectric boundary decaying into both materials, from [38]. 15

Figure 4. Two typical metamaterials in the microwave regime, a periodic structure equivalent to a homogenous medium and a non-periodic, gradient medium, from [19]. 16

Figure 5. (a) Depiction of metamaterial array of square resonators atop FR4. (b) Metamaterial dimensions and structure. 18

Figure 6. Overhead view of reflection data collection configuration. 19

Figure 7. Reflection data from 8 mm metamaterial. 21

Figure 8. Overhead view of antenna to antenna direct transmission measurement configuration. 21

Figure 9. Direct measurement - transmission power measured directly from antenna to antenna. 22

Figure 10. Reflection data from mirror and metamaterials of varying resonator size. 22

Figure 11. Reflection comparison for varying resonator array dimension sizes. 23

Figure 12. Absorption derived from raw reflection data. 24

Figure 13. Reflection data comparison with varying geometry. 25

Figure 14. Derived power values based on addition of components and phase shift. 27

Figure 15. Measured reflection and estimated values. 28

Figure 16. Fourier sine coefficient comparison for estimated metamaterial reflection data and the estimated transmitted power derived from measurements directly between antennas. 29

Figure 17. Measured reflection data and filtered data comparison. 30

Figure 18. Direct measurement and Fourier filtered data comparison. 31

Figure 19. Experimentally derived 8 mm metamaterial absorption. 32

Figure 20. Experimentally derived metamaterial absorption. 32

Figure 21. (a) Metamaterial unit cell. (b) Schematic representing boundary conditions for a plane wave at normal incidence, after [21]. 34

Figure 22. Metamaterial absorption comparison of experimentally derived data and model results. 36

Figure 23. Metamaterial absorber array where resonator dimensions control the detection frequencies and sensitivity is controlled by the thickness of the dielectric layer, after [5].....40

LIST OF ACRONYMS AND ABBREVIATIONS

AFRL	Air Force Research Laboratory
ASAT	Anti-Satellite Weapon
C3	Command, Control, and Communications
CRS	Congressional Report Services
DE	Directed Energy
DEW	Directed Energy Weapons
EM	Electromagnetic
EMS	Electromagnetic Spectrum
FE	Finite Element
GPS	Global Positioning System
HPM	High Power Microwave
KE	Kinetic Energy
KEW	Kinetic Energy Weapon
NEMA	National Electrical Manufactures Association
PCB	Printed Circuit Boards
PEC	Perfect Electric Conductor
PMC	Perfect Magnetic Conductor
PML	Perfectly Matched Layer
RF	Radio Frequency
RLC	Resistor, Inductor, Capacitor

THIS PAGE INTENTIONALLY LEFT BLANK

I. INTRODUCTION

After years of research and development, high-power microwave (HPM) weapons are becoming an operational reality [1]. These weapons have the potential to greatly increase the speed and effectiveness at which targets are prosecuted and may lead to completely new concepts of operations in warfare [1]. This technology is accessible to a wide range of potential adversaries [2]. High-power microwave weapons can be used to damage electronic components and disable critical communications networks [2]. Ultra large-scale integrated (ULSI) systems, very common in military systems, are particularly susceptible to HPM weapon attacks as failure rates are dependent on the size of transistor gates of the systems integrated circuits [3]. See Figure 1.

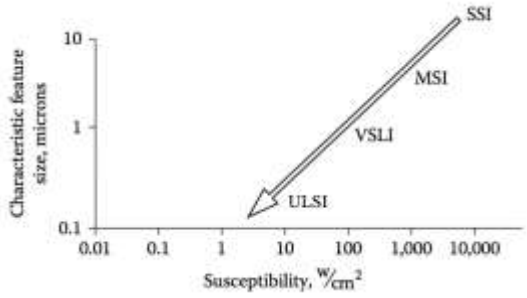

Figure 1. HPM susceptibility of integrated circuit technologies due to feature size, from [3].

Detection capability and characterization of energy from HPM weapons with metamaterials is the focus of this research. Metamaterials exhibit many unique characteristics, one of which is their absorption properties. The use of metamaterial absorbers in the THz frequency range has been demonstrated at the Naval Postgraduate School [4], and the results indicate flexibility and scalability, making this a viable approach in the microwave range [5]. A detector of microwave energy based on metamaterial absorbers has many potential applications, several of which are later discussed. The advantages of such a detector include affordability, simplicity, nearly limitless detection bandwidth and resiliency [5]. Microwave detection and characterization equipment currently exists. They consist of wide-band antennas, high-

gain pre-conditioning electronics, detection mechanisms, signal processing and data-storage circuitry and rely on large-scale integrated circuits, ironically making them susceptible to HPM attack and also complex and expensive [5]. The advantage of a metamaterial-based system is that the resonant frequency, i.e., the frequency to which the detector is capable of detecting is a function of the metamaterial physical dimensions. This allows for a matrix of detectors sensitive to different resonant frequencies, eliminating the need for bulky antennas and conditioning or signal processing electronics in existent electronic microwave receivers. The detection bandwidth is expanded simply by adding more detectors to the matrix. In the microwave regime, these detectors are on the scale of centimeters.

This research attempts to characterize the absorption of simple, inexpensive, commercially available metamaterials through experimentation. Experimental results are then compared with simulated results from a finite-element (FE) model to validate and refine the model for continued research. Potential detector designs and applications are discussed and future work is outlined.

II. HIGH POWER MICROWAVE WEAPONS OVERVIEW

High-power microwave weapons are a subset of a broader category of directed energy (DE) weapons. The U.S. Joint Publication on electronic warfare (JP 3–13.1) defines *directed energy* as

> an umbrella term covering technologies that produce a beam of concentrated electromagnetic (EM) energy or atomic or subatomic particles. A DE weapon is a system using DE primarily as a direct means to damage or destroy adversary equipment, facilities, and personnel. DE warfare is military action involving the use of DE weapons, devices, and countermeasures to either cause direct damage or destruction of adversary equipment, facilities, and personnel, or to determine, exploit, reduce, or prevent hostile use of the electromagnetic spectrum (EMS) through damage, destruction, and disruption [6].

Directed energy weapons (DEW) systems are generally categorized as:

- Lasers, which excite atoms to release photons in powerful bursts of coherent light
- High-power microwave/radio frequency (RF) weapons, which radiate electromagnetic energy in the high radio frequency (RF) spectrum
- Particle beam devices, which use large numbers of atomic or subatomic particles moving at relativistic velocities approaching that of light [7]

There has been considerable progress in directed energy technologies over the past two decades, and due to their use of the electromagnetic spectrum as the destructive mechanism, directed energy weapons have unique characteristics that will potentially enable new military operating concepts [1]. The movement toward directed energy weapons is considered one facet of the Revolution in Military Affairs occurring worldwide [1].

Directed energy travels at the speed of light. The challenge of tracking, computing intercept, and updating intercept solutions post weapons release for maneuvering targets is greatly reduced as the traverse time for the destructive mechanism is, for practical purposes, instantaneous. Additionally, there are no gravitational or atmospheric drag effects, nor are there kinematic or aerodynamic constraints to which traditional weapons

are subject. Complex ballistics are eliminated using directed-energy devices. Directed energy weapons are extremely precise and can accomplish surgical strikes [1]. Directed energy weapons are adaptable and flexible, primarily by changing the wavelength and power of their emitted energy to achieve desired effects.

The cost to engage targets with directed energy weapons is relatively inexpensive compared to conventional weapons. While the cost to develop, field, and maintain directed energy weapon is generally more expensive than traditional weapons systems, engagements are inexpensive as only energy is expended. In the case of missile defense, interceptor rockets, costing millions of dollars, are replaced by directed energy weapons that expend only thousands of dollars per engagement. Likewise, the directed energy weapons have the potential for deeper magazines, and thus, greater capacity for repetitive engagements over prolonged periods. Directed energy weapons are limited by power supply and dissipation of side effects (heat, chemicals, etc.) produced by beam generation compared to conventional weapons, which are limited by number of resupply rounds and space and weight limitations [1].

Another unique characteristic of directed energy weapons is their versatility for use as sensors. In the case of HPM weapons, they often operate in the same frequency as radars, giving them the detection and tracking potential in some applications [1].

An advantage that HPM weapons have over other DEW is low atmospheric attenuation, to include clouds, precipitation, and dust and small propagation loss [8], [9]. While HPM weapons require antennas to transmit electromagnetic energy, this energy spreads through diffraction and increases the weapons footprint to accommodate some lack of precision pointing required by lasers and particle beams [3].

HPM weapons are designed to disrupt and destroy targets by interfering, damaging or destroying electronics of the target. The development of sources capable of producing peak power in excess of a gigawatt [3] and the continuous breakthrough in key technologies in micro-electronics have made HPM weapons more relevant recently. Micro-electronics breakthroughs have resulted in weapons systems comprised of large-scaled and super high speed integrated circuitry [9]. The advent of solid-state electronics,

the continuous trend toward miniaturization, density, and power efficiency to accommodate this circuitry has made modern weapons systems more vulnerable to smaller amounts of microwave energy and thus HPM weapons a greater threat [3].

The term “high-power microwave weapons” refers to all directed energy weapons operating in the RF spectrum. There frequency range spans from 100 MHz to 100 GHz, with corresponding wavelengths of 3m to 3mm [9]. High power is generally accepted as meaning the source is able to generate of peak power of 100 MW [3].

There are two general categories of HPM weapons, narrow-band and wide-band, often referred to as ultra-wide-band, weapons.

Narrow-band weapons produce a modulated or damped sinusoidal waveform at a single frequency with a narrow bandwidth of only a few percent of the center frequency. In order to maximize the effectiveness of narrow band weapons, absorption characteristics of the target are desired to utilize the appropriate frequency. This may be achieved by scanning the target with a low energy source throughout the tunable frequency range and analyzing the reflected signals to determine target absorption. Not all narrow-band systems, however, are tunable. [10]

Wide-band weapon systems alleviate the need for target absorption characteristics by transmitting energy over a wide frequency band. The tradeoff is lower power transmission over the range of frequencies, but these systems are designed for use against a range of systems [10].

Both the wide-band and narrow-band systems share the same basic subsystem components common to all HPM weapon systems. They include:

- A prime power subsystem, which generates low-power electrical input in a long-pulse or continuous mode.
- A pulsed power subsystem, which takes the low power input from the prime power subsystem and converts it to high-power electrical pulses of much shorter duration.
- A microwave source, which transforms short duration, high-power electrical pulses into electromagnetic waves.

- A mode converter to tailor the spatial distribution of the electromagnetic energy to optimize transmission and antenna coupling.
- An antenna to direct the electromagnetic output into a high intensity beam [3].

In addition to these common components HPM weapons systems will have tracking, aiming and control systems [7].

HPM weapons are designed to disrupt the electrical components of a weapons system via electrical stimulation. Under electrical stimulation, conductive materials in the target act as antennae to the HPM energy and the transmitted energy couples with electrically conductive material stimulating electron flow, producing transient currents and voltages. Transient currents interfere with the normal operation of electrical components, inducing spurious signals that disrupt or damage sensitive components. Once introduced into a target, the system's own electronic circuitry transmits the pulse and causes damage deeper into the system [10]. At sufficiently high-power levels, these currents can produce electrical arcing across conductors and melting. When HPM energy enters a target the electromagnetic waves reflect multiple times within the system creating constructive and destructive interference resulting in regions of high and low electromagnetic field strengths. These regions can be many times stronger than the incident field exposing components situated at these nodes to even higher field strengths [11].

The Air Force Research Laboratory's (AFRL) Advanced Weapons and Survivability Directorate recognizes four major categories of electronic effects that can be produced by HPM energy: upset, lockup, latch-up and burnout [11].

- **Upset** is a temporary alteration of the electrical state of one or more nodes in such a way that they no longer function normally. Once the signal is removed, however, normal function returns with no permanent effects. Jamming is an example of this type of effect, where a sensor might lose lock because of interference.
- **Lockup** produces the same effects as upset, but an electrical reset is required to regain functionality, even after the signal is removed. If a computer were to freeze after exposure to an RF signal so that it had to be rebooted, this would be an example of lockup.

- **Latch-up** is an extreme form of lockup in which a node is permanently destroyed or electrical power is cut off to the node. A fuse blowing or transistors failing on a circuit board due to overloads from microwave radiation are two such examples.

- **Burnout** is the physical destruction of a node where the current becomes so great that conductors actually melt. This usually occurs within smaller wires or at junction nodes where multiple wires come together and often involves electrical arcing. The damage to household electronics caused by a lightning strike is an example of burnout.

In order to achieve these effects, the microwave energy must be transmitted into the electronics through circuitry pathways within the target. This is accomplished through either front-door or back-door coupling.

Front-door coupling is in-band penetration into the target circuitry through the targets' own antennas designed to receive signals in the microwave band such as communication antennas, radar antennas or altimeters. The radiation may be in-band or out-of-band with respect to the receiving system. In-band radiation is in the same frequency range as the target's antenna or sensor and will be amplified and passed directly through to the internal components. In-band, front-door coupling is the most efficient and destructive coupling method [12] but requires detailed target information. Out-of-band frequencies are outside of the antenna or sensors designed frequency range and will typically be filtered by the system. Out-of-band radiation may also couple with front-door receivers and produce effects on target; however, they do not couple as effectively [7].

Back-door coupling is less direct and refers to energy propagation into the target by any path other than antennas. Radiation may enter the through windows, vents, seams, seals, or cracks, solar cells, optical sensors, etc. Back-door coupling requires higher energy levels to induce performance degradation or damage but is typically more difficult to diagnose or eliminate [7]. Wide-band radiation is effective at back-door coupling because of the wide range of wavelengths involved, from 1 mm (gigahertz frequencies) to 3 meters (megahertz frequencies), which allows entry from multiple points [12].

High-power microwave weapons cause four levels (upset, lock-up, latch-up, and burnout) of destructive effect in electronic devices depending on the following:

- Distance to the target
- Vulnerability of the target
- Weapon frequency
- Generated power level and power density on the target
- Bandwidth
- Burst rate and pulse duration
- Dwell time on the target
- Coupling mode or entry points [7]

III. HPM WEAPONS APPLICABILITY IN SPACE

For roughly two decades, satellites have gained a pivotal role in modern conventional security and defense activities beyond their traditional strategic value. Consequently, they are considered new targets in military confrontations, and in recent years, potential advisories have demonstrated a renewed activity in the field of antisatellite researches and tests [13].

If there is a weakness to the United States' military dominance in the present era, it is reliance on satellites for space-based command, control, and communications (C3), and intelligence, surveillance, and reconnaissance (ISR) [8].

During testimony before the Senate Armed Service Committee in 2014, General William Shelton, Commander of Air Force Space command, stated: "We are so dependent on space these days. We plug into it like a utility. It is always there. Nobody worries about it" but "in space, our sustained mission success integrating these [satellite] capabilities into our military operations has encouraged potential adversaries to further develop counter space technologies and attempt to exploit our systems and information." [14] "Our nation's advantage in space is no longer a given. The ever-evolving space environment is increasingly contested as potential adversary capabilities grow in both number and sophistication" [15].

In February 2014, Director of National Intelligence James R. Clapper said potential adversaries were hard at work developing weapons that could degrade or destroy some of the United States' key satellites that provide essential communication to the military, the government and U.S. citizens [14]. "Threats to U.S. space services will increase during 2014 and beyond, as potential adversaries pursue disruptive and destructive counter-space capabilities," Clapper told the Senate Armed Services Committee. "Chinese and Russian military leaders understand the unique information advantages afforded by space systems and are developing capabilities to disrupt the United States' use of space in a conflict" [14]. According to a Congressional Research

Service (CRS) 1998 report addressing HPM devices, China's leaders view offensive counter space weapons as inevitable in future warfare [16].

In 2011 the Chinese journal *Modern Defence Technology*, whose target audience is Chinese senior military leaders, published the results of a feasibility study for the use of HPM weapons against satellite payloads. The study included key technologies and technology paths for HPM weapons, damage mechanisms and HPM coupling paths to satellite payloads. Through detailed numerical modeling of HPM coupling paths the study concludes satellite payloads can be effectively targeted by HPM weapons at the highest peak power levels or in close proximity to the target.

Directed energy weapons are already emerging. The Chinese are suspected of attempting to laser blind a U.S. NRO satellite in October 2006, and more recently, a Eutelsat satellite was purposefully jammed from a source in the Middle East [13].

Traditional anti-satellite weapons (ASAT) have been kinetic energy weapons (KEW), utilizing collision forces or explosive warheads to produce destructive effects. The United States fielded the first operational kinetic ASAT system in the 1960s, followed by the Soviets in the 1970s. Today, however, space is much more congested. KEW would add to the growing problem of space debris in crowed orbits. The resultant cloud of debris is extremely dangerous to other satellites as even a small piece of debris one cubic centimeter in size, could destroy a satellite [17]. In the end, consequences of any attack would not discriminate between the victim and the attacker [13].

In January 2007, China conducted its own KE ASAT by shooting down one of its own aging weather satellites. This resulted in 3,000 new pieces of on-orbit debris. The resultant backlash from the international community over this irresponsible creation of on-orbit debris, which will remain a hazard for decades, has been assessed as largely unexpected by the Chinese. This international pressure also acts as a deterrent to the use of KE ASAT weapons. This, and China's increased dependence on space, makes its use of KE ASATs less likely.

A. HPM WEAPONS AS ASATS

HPM weapons produce electronic kills. With the capability to disrupt, disable, or destroy critical electronic components of satellites, they do not produce space debris. While HPM weapons conceivably could attack satellites from a ground station, this would require a large rather-visible facility, with a powerful beam detectable through side lobes or grating lobes [8]. Attack from close proximity in a flyby encounter with single (or very few) HPM pulses would allow much lower power [8].

HPM weapons have the potential to provide scalable effects on targets. These weapons can temporarily deny the use of space assets or cause significant damage or even the destruction of satellites. In the case of communication satellites, a HPM device could interfere with the operation of satellite downlinks or operate directly against space-based electronic systems [1].

Another advantage of HPM weapons relates to the unlimited magazine capacity. Proposed space-based laser weapons use a limited magazine of chemicals to produce the laser beam, requiring replenishment or extremely limited use. While other types of weapons, including KEW, are "single-shot" devices, HPM weapons utilize electrical energy to produce the microwave emissions, and this energy can be obtained from variety of power sources, such as solar panels for a space-based system [17].

Another advantage of employing HPM weapons against satellites is deniability. Virtually no satellites, military or commercial, today possess attack warning and characterization sensors that would enable them to report they were under attack by a HPM weapon [1].

The application of directed-energy weapons technology with the greatest potential to change the conduct of warfare over the long term is in space [18]. They have the potential to become weapons of choice in the new space landscape [13]. The struggle for information dominance in future conflicts will require the ability to interfere with information collection and targeting and to prevent the transmission and processing of data. This means, in part, that adversaries will seek to deny the United States access to information from space-based surveillance systems and deny the ability to command,

control and communicate via space-based systems [1]. Undoubtedly, the earliest actions countering such weapons will be the most efficient [13]. Detection of HPM weapons is critical to defending from such attacks and characterize HPM weapons is fundamental to developing and implementing countermeasures.

IV. METAMATERIALS

The field of metamaterials and their applications is relatively new with increasing interest in the scientific and engineering communities over the past 15 years [19] with rapid progression [20]. Metamaterial is a broad term; there is no universally accepted definition of a metamaterial. However, common to all descriptions and definitions of metamaterials is that they exhibit properties not found in natural materials. These non-naturally occurring properties are the result of the metamaterials' electric and magnetic responses to incident electromagnetic radiation [21]. Electromagnetic waves contain both an electric field and a magnetic field. Each of these components induces a characteristic motion of the electrons in a material. Two parameters quantify the extent of these responses in a material: electrical permittivity (ε) quantifies how electrons respond to an electric field, and magnetic permeability (μ) quantifies the electrons' degree of response to a magnetic field [22]. Natural, or conventional, materials obtain their properties from individual atoms and molecules from which they are composed. When an electromagnetic wave travels through a material, the electrons within the material's atoms or molecules experience a force and resultant acceleration. The subsequent motion absorbs some of the wave's energy, affecting the properties of the wave and how it travels. By adjusting the chemical composition of a material, its wave-propagation characteristics can be altered.

Metamaterials offer alternative means to affect the electromagnetic response utilizing patterned structures, which are small relative to the wavelength of the incident radiation for which the metamaterial is designed. This possibility arises because the wavelength of a typical electromagnetic wave, the characteristic distance over which it varies, is orders of magnitude larger than the atoms or molecules that make up a material. The wave does not respond to an individual molecule but rather the collective properties of large numbers of molecules. Metamaterials replace the molecules with a structured architecture with dimensions dependent on the wavelength of the electromagnetic radiation for which the metamaterial is designed. See Figure 2. In a metamaterial, the

patterned elements are smaller than the wavelength and the wave response is due to the collective properties of these structures. In this way, properties are engineered through structure rather than mere chemical composition resulting in an effective permittivity and permeability based on chemical properties of the individual materials as well as the structure size [20].

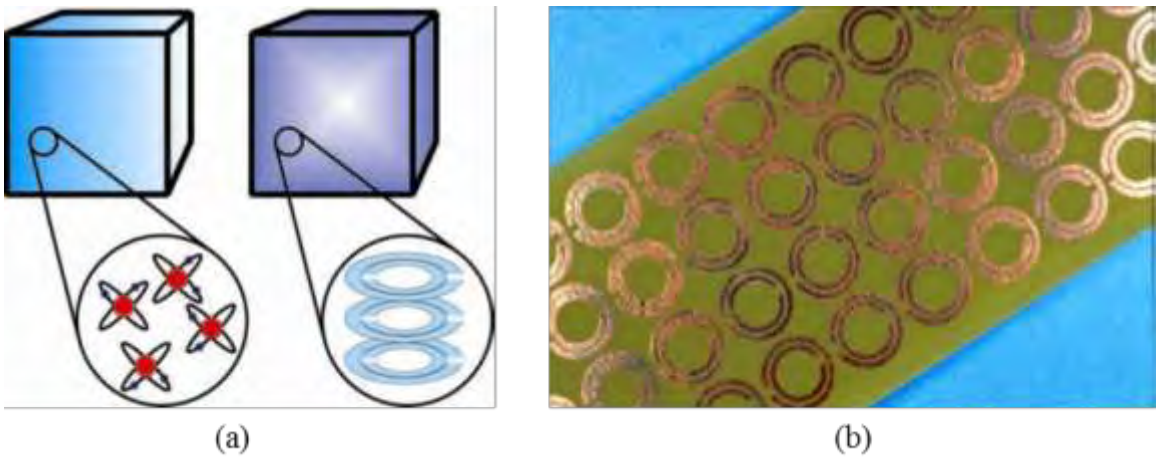

Figure 2. (a) In conventional materials ε and μ quantify how electrons respond to an electric field; in metamaterials, ε_{eff} and μ_{eff} are derived from the patterned elements which may contain many atoms. (b) An early example of a metamaterial with a resonant magnetic response. Split rings are etched onto a circuit board, from [20].

Absorption is one such property that can be engineered to achieve non-naturally occurring characteristics beneficial to applications such as radiation detection. Near perfect metamaterial absorbers have been realized over limited frequency bands, dependent on the metamaterial subwavelength features. These resonant absorbers have been realized across the electromagnetic spectrum [23]–[36].

Metamaterial absorbers are typically composed of a periodic-patterned metal layer, a dielectric spacer and a ground plane [23]–[36]. Under the right circumstances, incident electromagnetic radiation at interfaces between metal and dielectric induces a resonant response. That resonant reaction occurs between the incident radiation and the free electrons at the surface of the metal, i.e., the frequency of oscillation of the free

electrons in the surface of the metal correspond to the frequency of incident electromagnetic radiation [37]. The result is the generation of surface plasmons—density waves of electrons that propagate along the interface like the ripples that spread across the surface of a pond after you throw a stone in the water" [37]. (See Figure 3.) These waves decay exponentially into both the metal and dielectric [38]. As incident electromagnetic radiation induces these surface plasmon resonances, the resultant resistive losses in the metal and additional losses in the dielectric layer convert incident energy to heat, allowing absorption of the incident radiation.

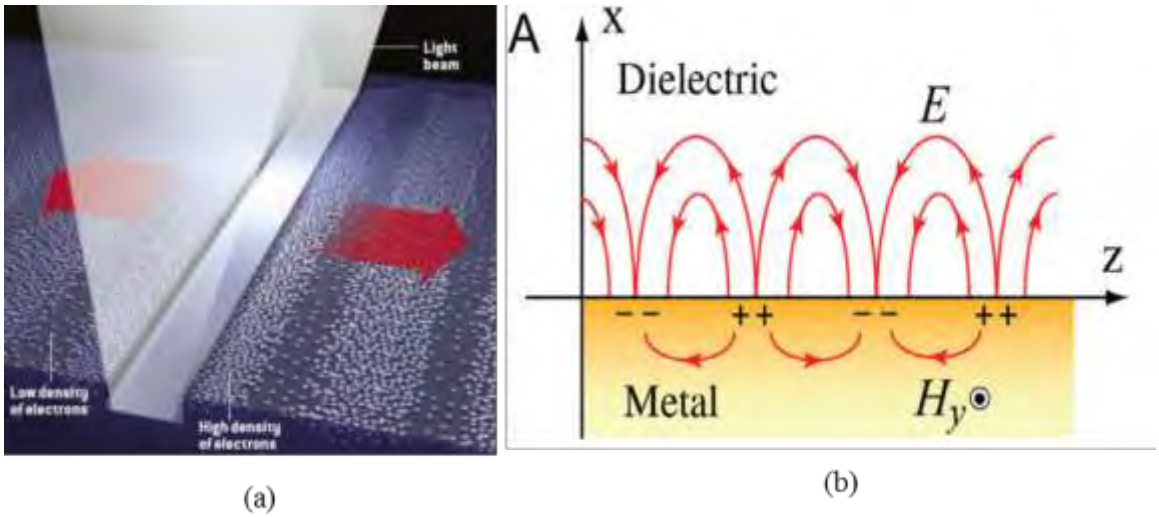

(a) (b)

Figure 3. (a) Plasmons flow along the boundary between a metal and a dielectric. Light incident to the grove in a metal generates plasmons that propagate along the metal surface (boundary between metal and air), from [37]. (b) Surface plasmons propagate along the metal/dielectric boundary decaying into both materials, from [38].

In theory, metamaterials can be fabricated for any frequency by varying the geometry of the structure. This tuning is only weakly dependent on the materials used allowing construction using mature microfabrication and printed circuit board (PCB) techniques [39]. While a variety of materials can be used, the materials do have a significant impact on optimal dimensions for metamaterial geometry. Metals, or equivalent highly conductive materials, require sufficient thickness and conductivity to

function as resonators. The refractive index of the dielectric is also significant and will affect optimal absorption frequencies [39].

These composite structures with macroscopic cellular structures may be periodic or non-periodic. A metamaterial with periodic structures is equivalent to a homogenous medium while non-periodic metamaterials are equivalent to inhomogeneous, or gradient, mediums. Figure 4 illustrates typical periodic and non-periodic microwave metamaterial structures. Sub-wavelength split ring resonators, on the order of 10s of millimeters as illustrated, are used to create structures that have simultaneous negative permittivity and permeability. This non-naturally occurring property is particularly applicable to microwave patch antenna design allowing antenna miniaturization and increased directivity gain [40]. These types of structures also have applications for filters [41], waveguides [42], and frequency selective surfaces [43]. Figure 4 (b) illustrates a gradient medium. In this type of structure, because the concentration of resonators is a function of the radial distance from the center of the material, so too is the electrical permittivity and the refractive index. This type of structure that produces a gradient index of refraction has applications for Luneburg lens design to alleviate aberrations [44].

These metamaterial structures are typically comprised of a non-ferrous conductive material and a dielectric. Periodic structures are often described by a single component of their cellular structure referred to as a unit cell.

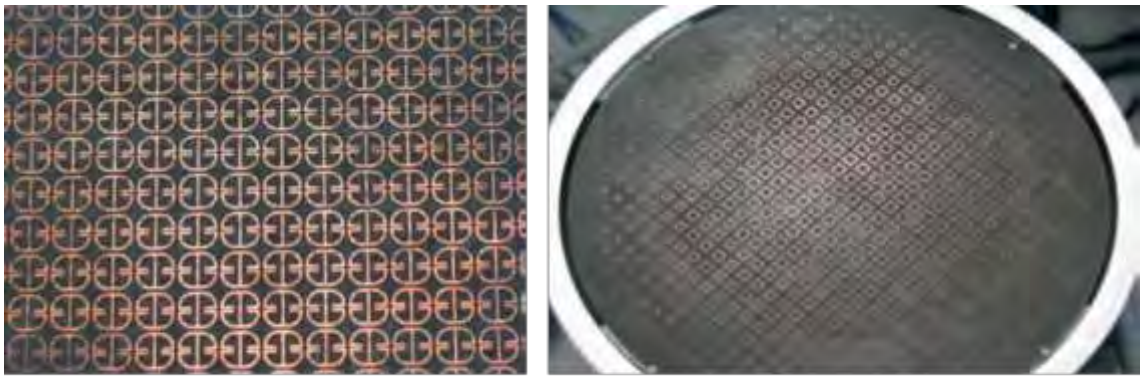

Figure 4. Two typical metamaterials in the microwave regime, a periodic structure equivalent to a homogenous medium and a non-periodic, gradient medium, from [19].

V. EXPERIMENTAL DATA COLLECTION AND ANALYSIS

The experimental portion of this study sought to demonstrate that simple metamaterial structures could be utilized as absorbers and tuned for specific frequencies in the microwave region. The method used was to radiate microwave energy through a directional antenna towards pre-fabricated metamaterial structures measuring the reflected energy. This was then repeated for a perfect reflector of the microwave energy. Comparing the reflected energy data of the two allowed calculation of the absorption of the metamaterial structures. Both the reflection data and the derived absorption data contained unexpected periodic oscillations, referred to as "fringes," that were determined to be a result of wave interference. The wave interference was a result of energy reaching the receiving antenna through two separate paths. The primary, and intended path, was from the transmitting antenna, reflecting from the metamaterial, to the receiving antenna. The secondary path was directly from the transmitting antenna side lobe to the side lobe of the receiving antenna. This multipath interference effect was filtered by use of a discrete Fourier transform.

This chapter describes the metamaterial structures, the experimental configuration and data collection method. The derivation of the absorption from the reflection data is detailed and the wave interference and resultant fringes are discussed as well as the methods used to determine the source of fringes and verify it. The filtering method for the removal of the fringes is discussed and validation of this method is presented. Finally, the absorption data of the metamaterial structures are presented.

A. METAMATERIAL STRUCTURES DESCRIPTION

Metamaterial absorbers studied were simple composite structures consisting of a copper ground plane and square copper resonators separated by an FR4 dielectric layer. The resonator squares atop the FR4 were fabricated in uniform row and column arrays with 1 mm separation between squares. See Figure 5 (a). These metamaterial structures were manufactured using standard PCB fabrication process, which was selected because of its availability and affordability. Resonator sizes were 8, 9, and 10 millimeters,

approximately a quarter wavelength of the target resonant waves. The resonator and ground plane thickness (30 μm) were determined through optical profilometer measurements and the accurate value for dielectric thickness (to later be used in the finite element model) was deduced from the total thickness of the material and metal films. The fabrication process resulted in over etched regions between the resonators. The depth of the over-etched region was also determined by optical profilometer measurement (230 μm). The structure profile and dimensions are detailed in Figure 5 (b).

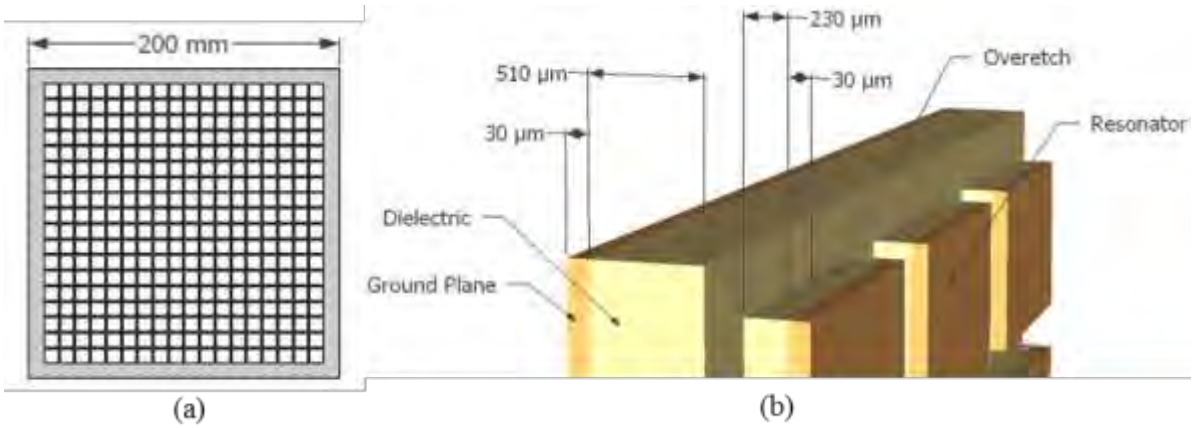

Figure 5. (a) Depiction of metamaterial array of square resonators atop FR4. (b) Metamaterial dimensions and structure.

B. DATA COLLECTION

Experimental data were collected in a 15×5 meter anechoic chamber utilizing a wave generator, spectrum analyzer and transmitter and receiver antennas. The transmitting and receiving antennas were positioned symmetrically about the reflecting surface, as illustrated in Figure 6, to maximize reflected energy at the receiver antenna.

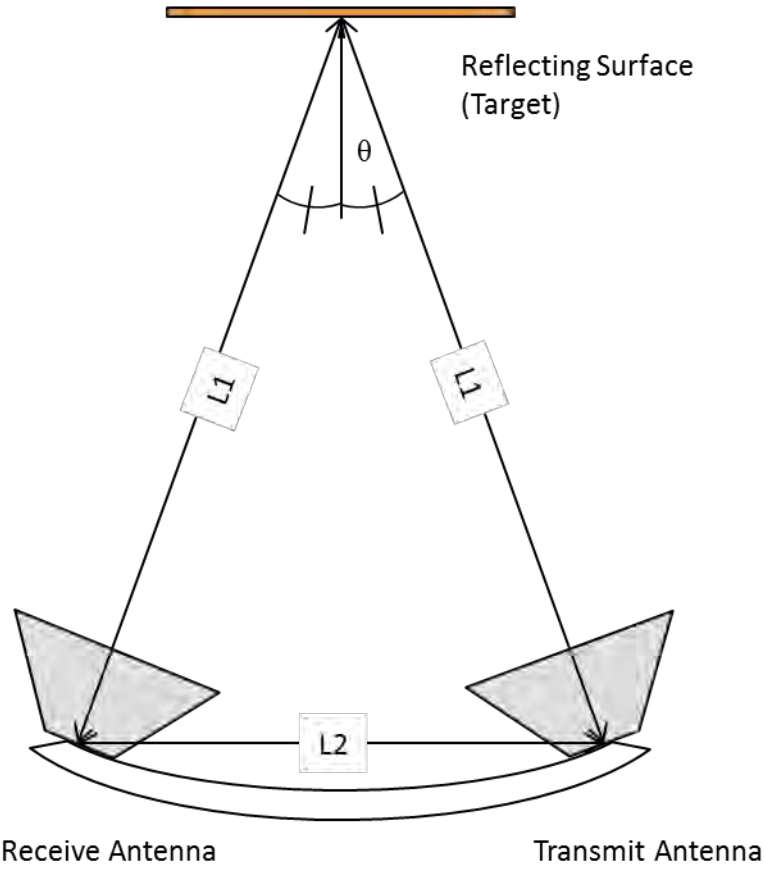

Figure 6. Overhead view of reflection data collection configuration.

The distance L_1 varied from 0.635 to 1.10 m while L2 was 0.33 m. Identical 5 inch horn receiving and transmitting antennas were used rated for 2 to 13 GHz. Absorption of microwave energy by the metamaterial structures was determined by comparing reflected energy from the metamaterial structures to that of a mirror. A copper sheet with matching overall dimension of the metamaterial structures was used as the mirror and assumed to be a perfect reflector for this frequency range, i.e., all the incident radiation was reflected. . This measurement was used to establish 100% signal strength. Directed microwave energy was swept through the designated frequency range of 5 to 13 GHz, corresponding to wavelengths of 2.3 to 6.0 cm, and the maximum reflected power was collected and recorded at 401 discrete frequencies for both the metamaterial structures and the mirror. As the mirror was assumed to be a perfect reflector and therefore the reflected energy from the metamaterial structure can be assumed equal to or

less than the reflected energy from the mirror, the reflectance of the metamaterial (R), with values from 0 for no reflection to 1 for 100% reflection, can expressed as a ratio of the power received from the reflection from the metamaterial structure $(P_{metamaterial})$ to the power received from the reflection from the mirror (P_{mirror}). In the same relative terms, absorptivity (A) can be expressed in terms of reflectance (R) and transmittance (T):

$$A = 1 - R - T \tag{1}$$

Assuming no transmission since the copper ground plane thickness is greater than the skin depth and replacing the reflectance term with the reflection power ratio, the absorptivity, A, for the metamaterial is:

$$A = 1 - \frac{P_{metamaterial}}{P_{mirror}} \tag{2}$$

C. DATA ANALYSIS

Examination of the reflection data reveals interference fringes in both of the reflected energy spectra (from the mirror and from the metamaterial structures). These fringes are apparent in Figure 7, which shows the reflection data from the 8 millimeter metamaterial structure.

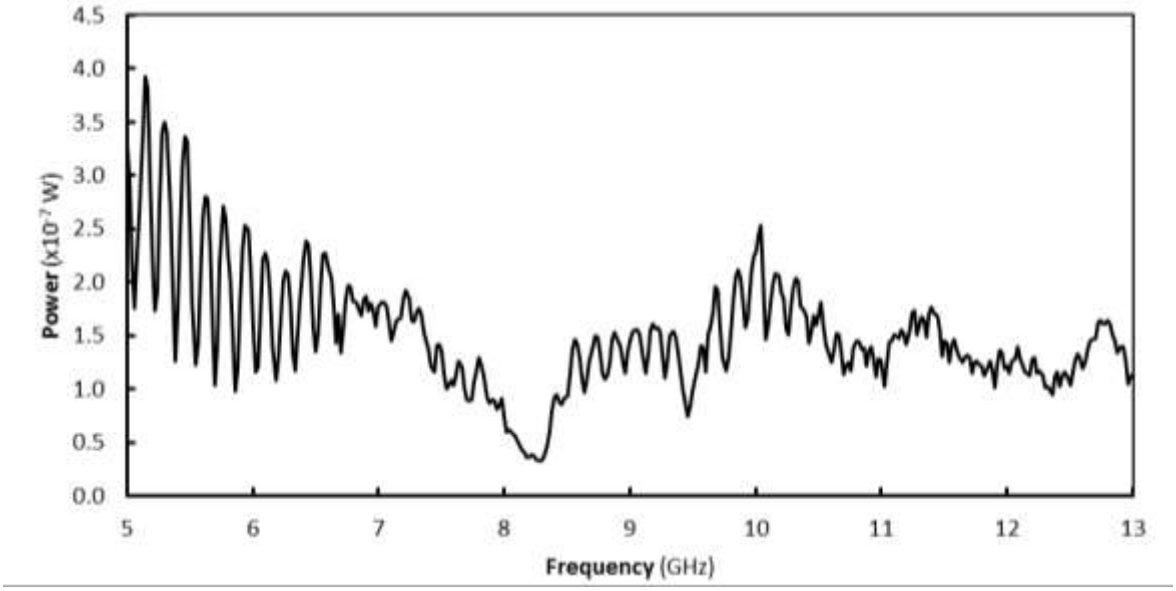

Figure 7. Reflection data from 8 mm metamaterial.

Sweep and scan rates were varied on the wave generator and spectrum analyzer to verify they were not contributors to this fringing effect. In order to verify that the fringes were not produced by the wave generator itself, the power of the generated waves was measured directly from the transmitting antenna to the receiving antenna as illustrated in Figure 9. Figure 9 shows the transmission power data from this measurement. The fringing effect is notably absent in this direct measurement.

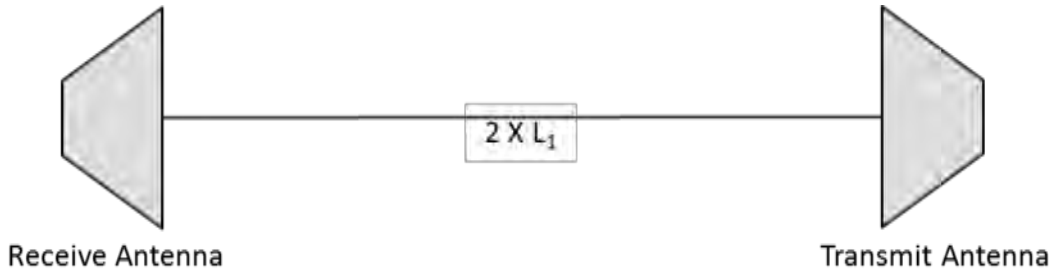

Figure 8. Overhead view of antenna to antenna direct transmission measurement configuration.

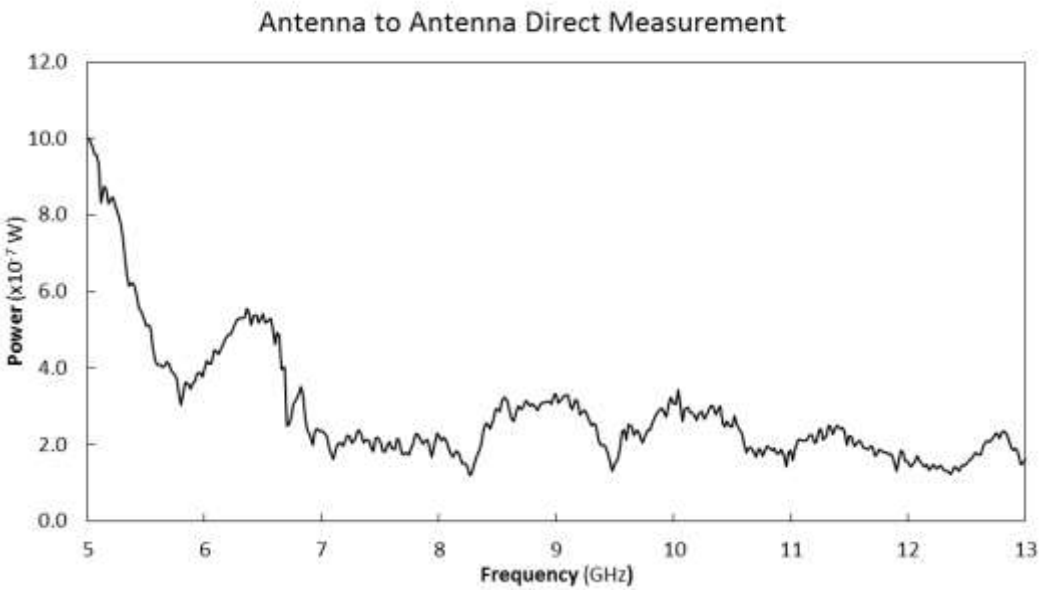

Figure 9. Direct measurement - transmission power measured directly from antenna to antenna.

The fringes in the reflected power occur for both the mirror and the metamaterials and are independent of the resonator size of the metamaterial as evident in Figure 10.

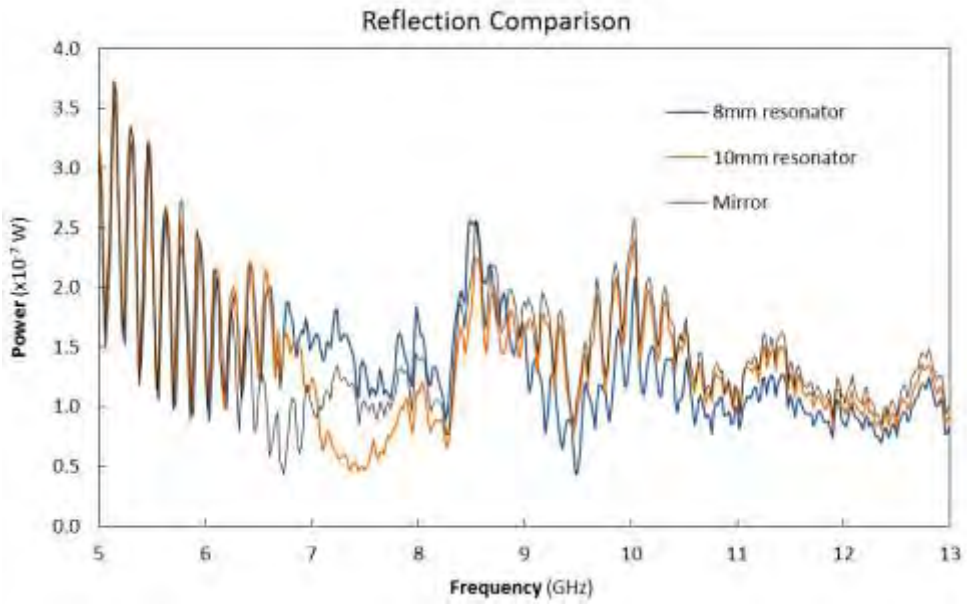

Figure 10. Reflection data from mirror and metamaterials of varying resonator size.

The fringes in the data are also independent of the overall metamaterial dimensions. Figure 11 compares two metamaterials constructed of 8 millimeter resonators, one with a 20×20 resonator pattern and the second an 8×8 resonator array.

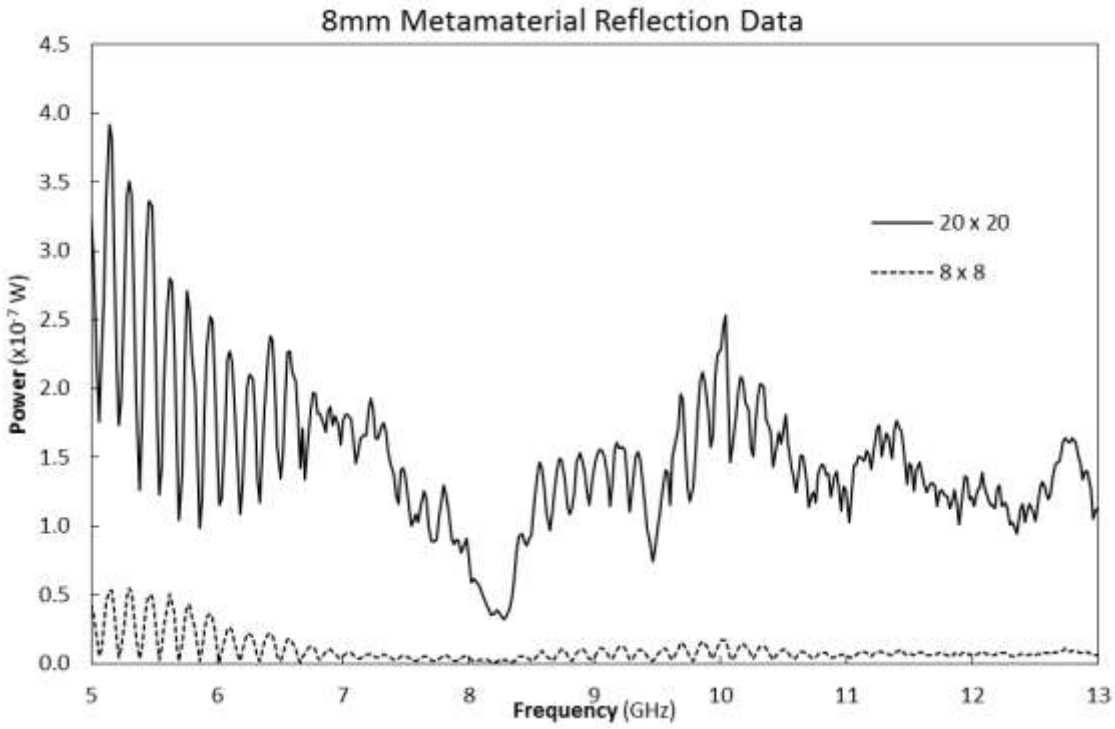

Figure 11. Reflection comparison for varying resonator array dimension sizes.

The fringes are, however, dependent on the geometric configuration of the measurement system antennas and the reflecting surface. We have determined that this occurs because the fringes are the result of multipath wave interference between the energy reflected from the metamaterial (along the primary path) and the undesired energy transmitted directly antenna to antenna through antenna side lobes. This interference also introduces fringes in the derived absorption with the same periodicity as evident in Figure 12.

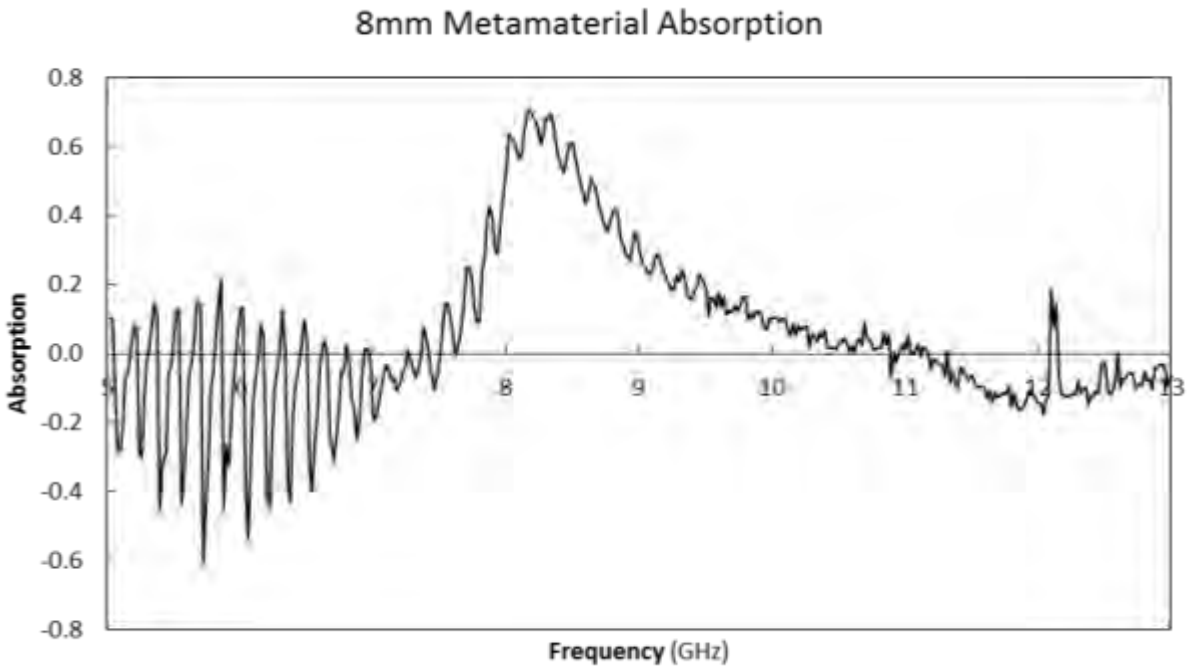

Figure 12. Absorption derived from raw reflection data.

Varying the geometric configuration of the antennas and reflecting surface varies the difference in the two separate paths, the energy travels between antennas, thus changing the wave interference pattern and fringe effects. Figure 13 demonstrates this effect. Here the distance L_1 and angle θ depicted in Figure 6 were varied with L_1=1.10 m for one configuration and L_1=0.635 m for the second configuration. For L_1=1.10 m, which is the same configuration for the data presented in Figures 7, 10, 11, and 12 the average peak separation of the interference fringes is 158.3 MHz. Changing the configuration by decreasing L_1 to 0.635 m, yields an average peak separation of 322.2 MHz between subsequent fringes.

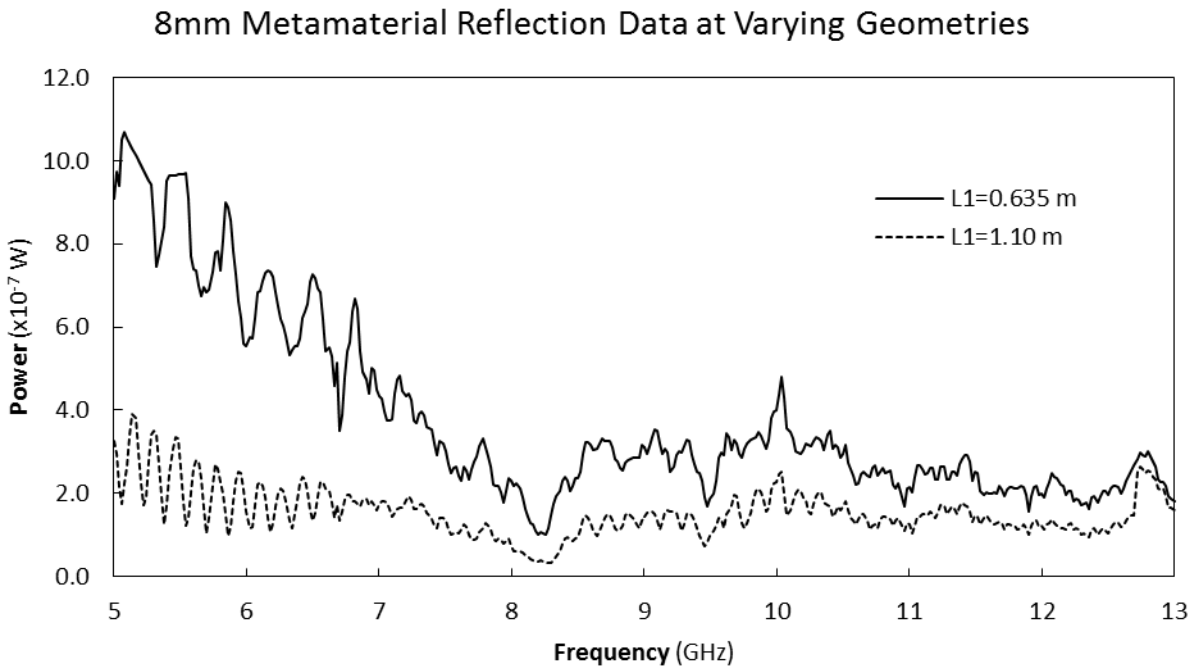

Figure 13. Reflection data comparison with varying geometry.

The frequency of this induced fringing imbedded on the reflected energy is predictable based on the geometry of the antennas and reflecting surface. Examining Figure 7, the reflected energy travels a distance $2L_1$ from the transmitting antenna to the receiving antenna. Energy reaching the receive antenna through side lobes travels a distance of L_2. Let Δd define the difference in distance traveled, and λ represent wavelength. These are related by:

$$\Delta d = 2L_1 - L_2 \tag{3}$$

$$\Delta d = n\lambda \tag{4}$$

When the difference in the distance the energy travels is an integer multiple of the energy's wavelength, i.e., n has an integer value in Equation (4), then the phase shift of the incoming waves will be eliminated and the maximum constructive interference will occur.

Using the relationship $f = \frac{c}{\lambda}$ and substituting with Equations (3) and (4):

$$f = \frac{nc}{2L_2 - L_1} \tag{5}$$

Therefore the induced interference fringe *frequency* (separation between n^{th} and $(n+1)^{th}$ fringe) is:

$$\Delta f = \frac{c}{2L_1 - L_2} \tag{6}$$

Substituting with the values from the experimental configuration for L_1 and L_2

$$\Delta f = \frac{c}{2L_1 - L_2} = \frac{2.998 \cdot 10^8 \frac{\cancel{m}}{s}}{\left(2 \cdot 43.5 \cancel{in} - 13.5 \cancel{in}\right) \cdot \frac{.0254 \cancel{m}}{1 \cancel{in}}} = 160.6 MHz \tag{7}$$

$$\Delta f = \frac{c}{2L_1 - L_2} = \frac{2.998 \cdot 10^8 \frac{\cancel{m}}{s}}{\left(2 \cdot 25 \cancel{in} - 13.5 \cancel{in}\right) \cdot \frac{.0254 \cancel{m}}{1 \cancel{in}}} = 323.4 MHz \tag{8}$$

These predicted results confirm the values determined from experimental data. If the experimental reflectance spectrum is assumed from the ideal (no cross-talk) signal and experimental measurements of cross-talk signal alone, this oscillation can be also be replicated by the relationship:

$$P_{meas} = \left(\sqrt{P_{refl}} + \sqrt{P_{SL}} \cdot \sin\left(\frac{\left(2L_1 - L_2\right) \cdot f}{c} \right) \cdot 2\pi \right)^2 \tag{9}$$

where P_{meas} is the measured power being replicated, P_{refl} is the power of the reflected energy from the metamaterial, and P_{SL} is the power of the energy received directly from antenna to antenna through side lobes. The sine term accounts for the phase difference between reflected energy and energy reaching the antenna through the side lobes.

The power received through the side lobes alone, P_{SL}, was measured by removing the reflecting surface from its position indicated in Figure 7 and recording the received power in the anechoic chamber. The direct antenna to antenna measurement previously

described and depicted in Figures 9 and 10) was used to represent ideal, interference-free reflected energy, P_{refl}. Evaluating Equation 8 with this data and the L_1 and L_2 values used experimentally allows a solution for the predicted power measurement. This predicted power measurement (Figure 14) contains the same oscillation of approximately 160 MHz found in the experimental measurements.

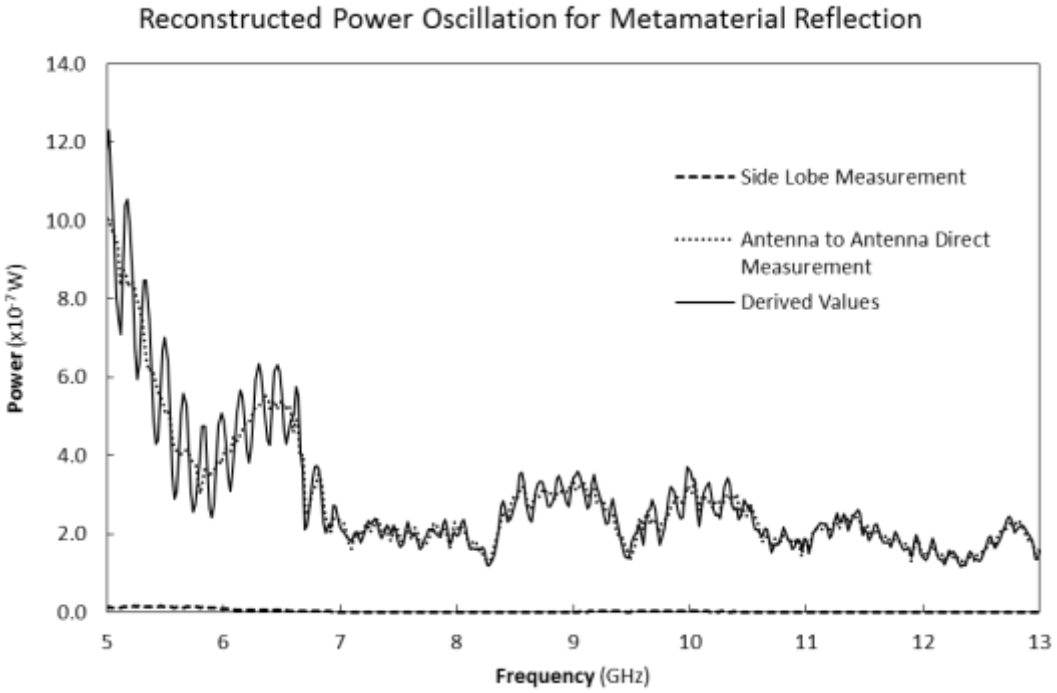

Figure 14. Derived power values based on addition of components and phase shift.

While this relationship (Eq. 9) was effective for predicting the interference, it proved inadequate to remove the effects of the interference to obtain accurate reflection data. This is due to the limitation in spectral resolution of the spectrum analyzer. In order to remove the effects of the interference from the reflection data a technique from signal processing was adopted. The reflection data, the signal obtained from reflections from the metamaterial structure was estimated via discrete Fourier transform. Figure 15 shows the high correlation between this estimated signal and the actual data.

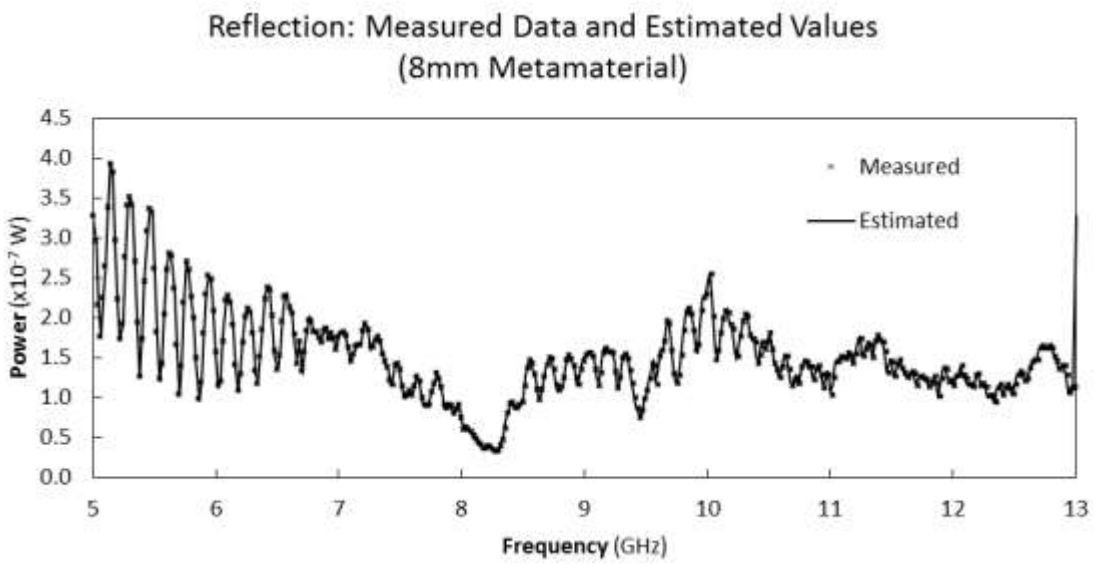

Figure 15. Measured reflection and estimated values.

Similarly, an estimated, ideal, interference-free signal was derived for the data obtained from the direct antenna to antenna measurements void of this induced oscillation via discrete Fourier transform. The geometric form of the Fourier transform was used to generate these estimated signals that are well correlated to the actual signals. Figure 16 compares the sine coefficients of the Fourier transforms for the estimated metamaterial reflected signal and the interference-free signal.

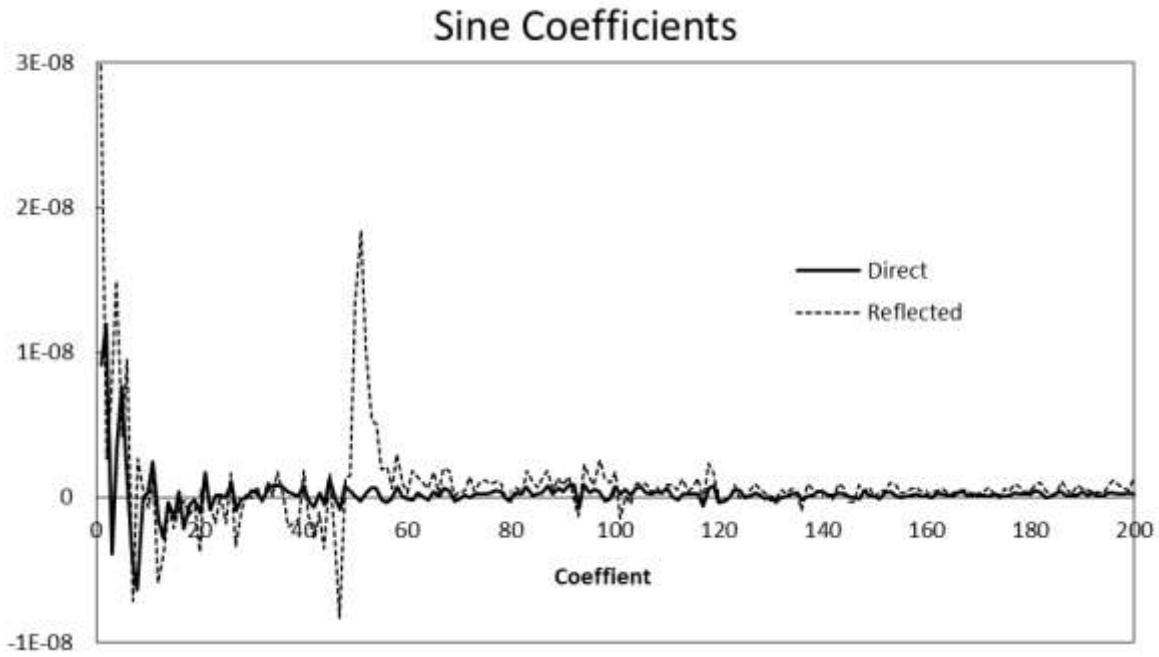

Figure 16. Fourier sine coefficient comparison for estimated metamaterial reflection data and the estimated transmitted power derived from measurements directly between antennas.

The effect of the wave interference in the reflected signal is apparent as coefficients 41–61 diverge from the coefficients derived from the interference free direct measurement. The center coefficient in this divergent range corresponds to a frequency of 157 MHz, which correlates with the observed fringe oscillation in the raw data evident in Figure 8 and the fringe oscillation present when the power predicted measurement was based on wave interference in Figure 14. By removing these coefficients the fringing effect of the wave interference is filtered. Figure 17 compares the raw reflection data and the filtered data with these coefficients removed.

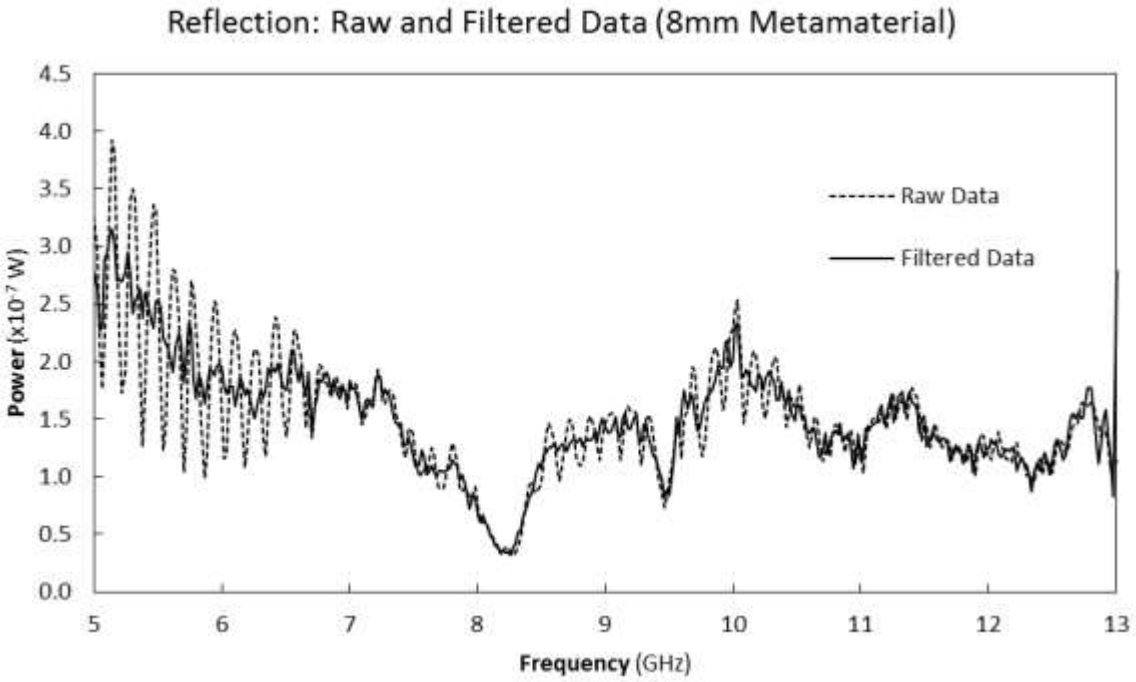

Figure 17. Measured reflection data and filtered data comparison.

To validate this filtering method it must be applied to a signal with interference fringing and then comparing the filtered result to the interference-free signal. To accomplish this, the interference-free transmitted power data obtained by the direct antenna to antenna measurement previously discussed and illustrated in Figures 8 and 9 was used as the interference-free signal. Interference fringes were introduced by the addition of the received side lobe energy in accordance with Equation 8 and depicted in Figure 14 as the derived values. The discrete Fourier transform was then applied to these derived values to obtain the estimated signal inclusive of the fringe effects. The same divergent coefficients previously identified as divergent, were then removed to filter the interference fringes to generate an estimate of the original interference-free signal. This filtered estimate is compared to the original measured transmitted power data measured directly from antenna to antenna in Figure 18.

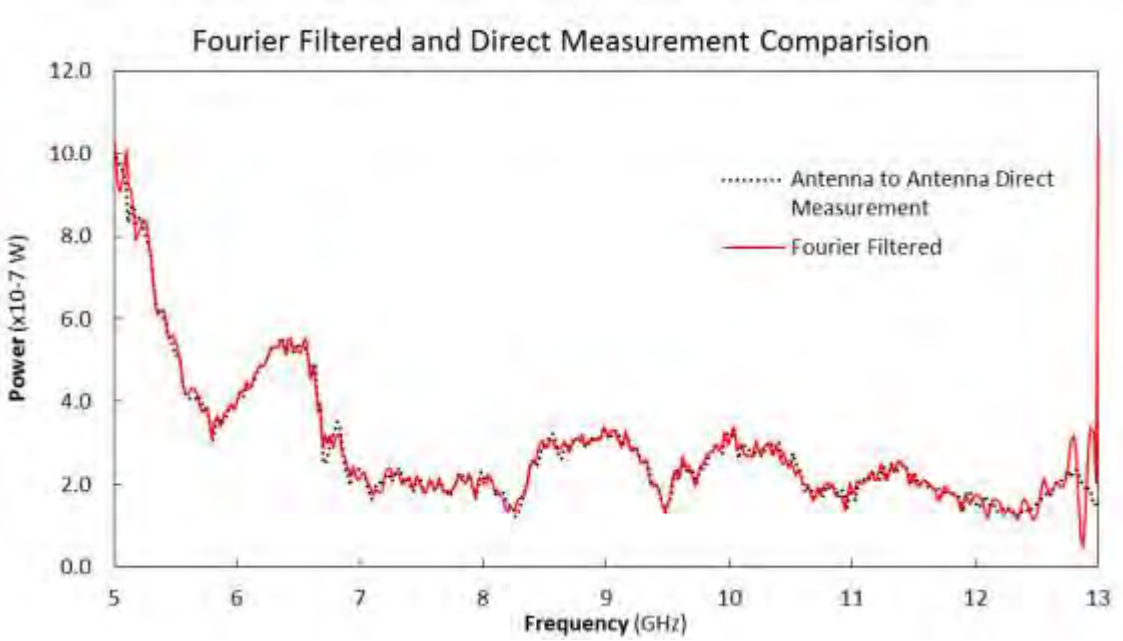

Figure 18. Direct measurement and Fourier filtered data comparison.

Figure 19 shows the resultant absorption plot when applying this same filtering method to both the mirror and metamaterial reflection data and calculating absorption via Equation (2). Likewise, this methodology was applied to obtain the absorbance of 9 mm and 10 mm metamaterials, which are displayed in Figure 20. In both figures fringing effects are reduced but some effects remain due to the limited number of data points in the data.

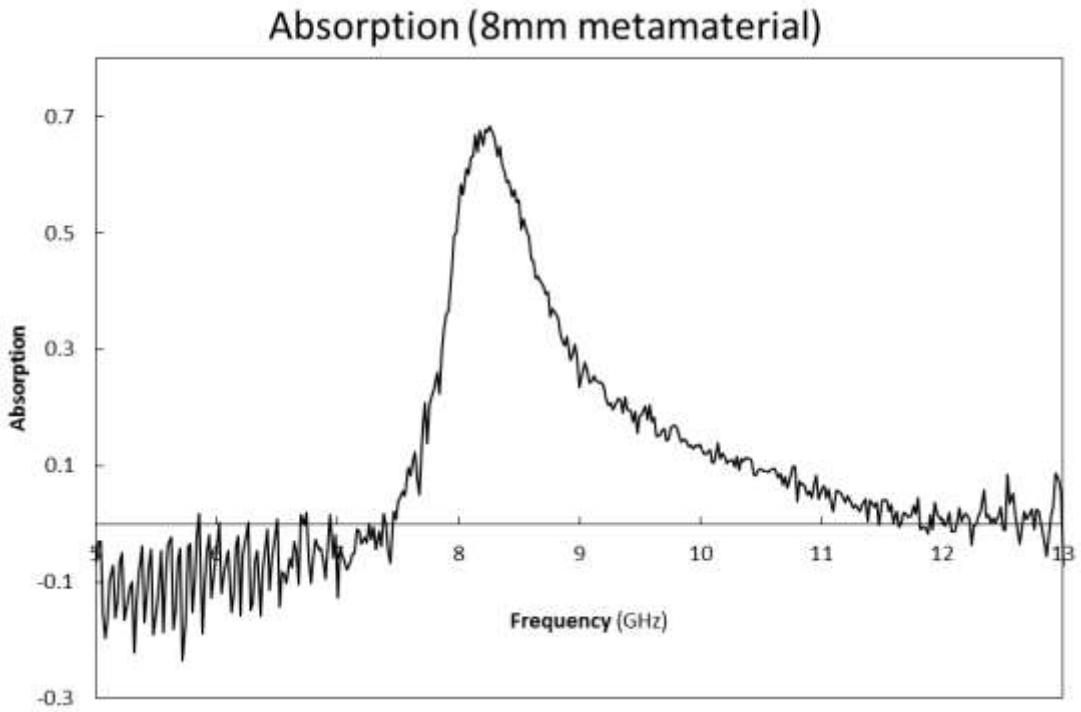

Figure 19. Experimentally derived 8 mm metamaterial absorption.

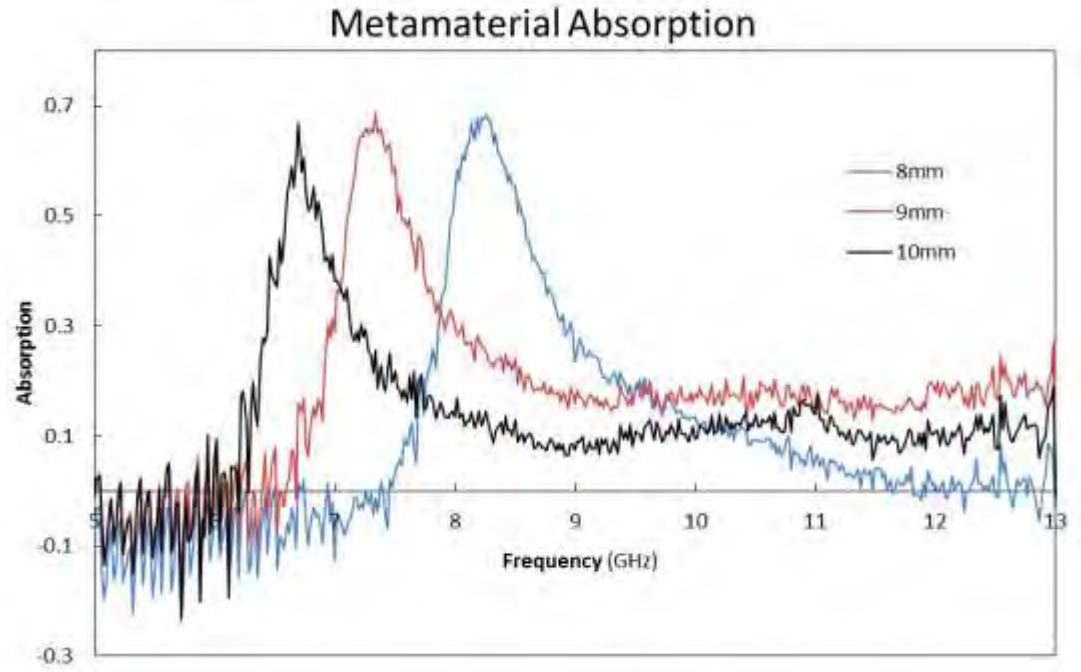

Figure 20. Experimentally derived metamaterial absorption.

VI. MODELING

Experimental data is essential to evaluate the properties of metamaterials; however, numerical modeling can effectively predict the properties of a metamaterial absorber eliminating the need to fabricate every potential combination of material composition and geometric configuration.

The model used to simulate the absorption characteristics in this study was developed by B. Kearney [39] to investigate absorption characteristic of metamaterials in the terahertz region. The model was adapted for the microwave regime by modifying the geometry and material properties to match particular metamaterials in this study.

The resonant absorption frequency and magnitude of absorption can be derived and explained using a number of theoretical explanations such as impedance-matching to free space [21], an equivalent resistor inductor capacitor (RLC) circuit [45], [46], confined TM cavity modes [47], interference of multiple reflections [48], and transmission lines [49]. Due to the complexity of metamaterials they are typically simulated by FE models [45]–[49]. Therefore, understanding numerical models of metamaterials is essential to accurately predict their properties.

Finite element analysis was used to model the absorption characteristics of the fabricated metamaterials, for comparison to the experimental data, with COMSOL multi-physics software.

It is important that the geometry and material properties be replicated as accurately as possible to match the fabricated structure, as minor changes may lead to variations in absorption characteristics. The thicknesses of the FR4 dielectric, the copper resonators and ground plane, and over-etched regions were modeled according to the measurements previously described. The bulk value $\left(\sigma = 5.8\times10^{7}\ S/m\right)$ was used for the conductivity of copper [50] and the FR4 was modeled with a relative permittivity of 4.4 and with a loss tangent of 0.02 [50].

Appropriate boundary conditions and meshing are critical factors in a FE model. To simplify the model, the periodic structure of metamaterial can be exploited as any electromagnetic solution must satisfy periodic boundary conditions. Accordingly, only a single unit cell of the metamaterial with appropriate periodic boundary conditions is necessary for FE analysis (Figure 21).

The COMSOL radio frequency module allows the simulation of an incident plane wave of microwave radiation into a surface using scattering boundary conditions or plane wave generation on a boundary using internal ports.

In this analysis the assumption of incident radiation normal to the metamaterial surface was made. Under such circumstances, the electric and magnetic fields of the incident plane wave can be broken into two polarizations with fields normal to the boundaries. In this case, a perfect electric conductor (PEC) will enforce periodic boundary conditions for electric fields normal to the boundary, while a perfect magnetic conductor (PMC) will enforce periodic boundary conditions for magnetic fields normal to the boundary [39].

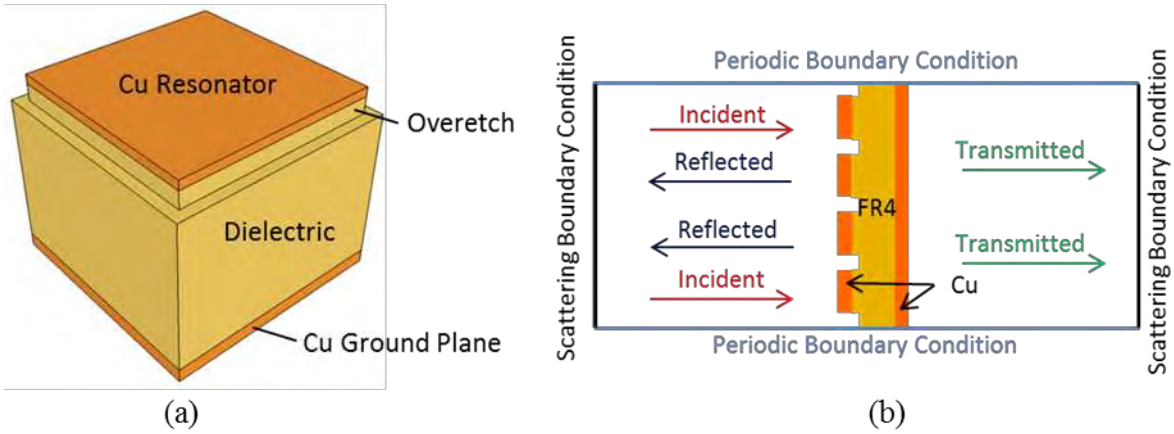

Figure 21. (a) Metamaterial unit cell. (b) Schematic representing boundary conditions for a plane wave at normal incidence, after [21].

Appropriate boundary conditions must be set to allow accurate modeling of incoming, reflected and transmitted radiation incident to the metamaterial. On the incoming side, a surface must exist that generates, or allows the penetration of, the incident radiation

and then, for the reflected radiation from the metamaterial either absorbs that reflection or allows it to leave the model, in either case without allowing radiation to re-enter through secondary reflections. A second surface, opposite the ground plane, must allow any transmitted radiation to leave the model or absorb it, also without allowing radiation to reflect back into the model. Several methods available in COMSOL are scattering boundary conditions, internal ports, and perfectly matched layers (PMLs) 41].

Scattering boundary conditions approximate an infinite space or "open" boundary for radiation to propagate out through. They act as first order absorbing boundary conditions for plane, cylindrical, or spherical waves. Similarly, port boundary conditions allow perfectly absorbing boundary conditions for general modes of known shape. Both of these boundaries also can allow wave to penetration into the model, supplying the incident radiation [39].

While not exactly a boundary condition, a PML can be used to approximate an open boundary. A PML is similar in function to an ideal metamaterial absorber; it is impedance matched to the material to which it is adjacent and can eliminate reflection. It uses a complex coordinate transformation to cause incident electromagnetic waves to decay as they propagate resulting in essentially total absorption [51]. The PML has a finite thickness and must have additional mesh elements and should be coupled with a scattering boundary condition to minimize back reflections [39].

A schematic for the boundary condition setup in this study is shown in Figure 21 (b). Due to the thickness of the copper resonators and ground plane greater than the skin depth (approx. 0.5 to 0.9 micron) the transmitted energy in this model is zero.

Once geometry is replicated, boundary conditions set, and mesh applied, the wave equations for the model to solve must be specified. The default option for COMSOL and the optioned applied for this simulation is "relative permittivity" equation, which solves the EM wave equation of the form:

$$\nabla \times \mu_r^{-1} \left(\nabla \times \vec{E} \right) - k_0^2 \left(\varepsilon_r - \frac{j\sigma}{\omega \varepsilon_0} \right) \vec{E} = 0 \tag{10}$$

This equation is useful for materials that can be defined entirely by permeability and permittivity, such as free space, or those where conductivity dominates, such as most metals in the microwave regime.

Once the model construction is complete solvers are chosen. This analysis utilized a frequency domain solver, which simply solves the EM wave equations at specified frequencies. Additionally, parametric sweeps were utilized to vary to unit cell dimensions to replicate the fabricated metamaterial sizes. Finally, once the model has finished its run, results yield the E and B-field solutions allowing for additional derived values, in this case absorption. When magnetic losses are negligible the absorption characteristic can be extracted by performing volume integrations of the resistive losses in the metamaterial. Non-linear effects are largely ignored in these models, so as the incoming power was established at 1 W and the absorption is represented as Watts of power absorbed in the metamaterial. Figure 22 compares the model derived absorption and experimentally determined absorption of the metamaterials.

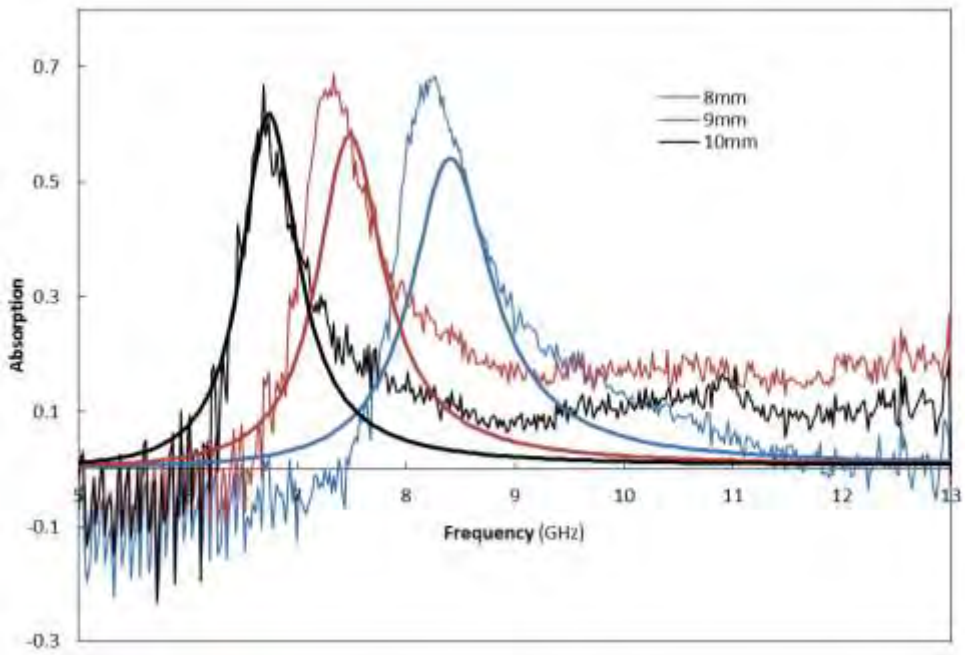

Figure 22. Metamaterial absorption comparison of experimentally derived data and model results.

VII. CONCLUSIONS

A. SUMMARY OF RESULTS

Experimental and modeled results both confirm metamaterial absorbers can be tuned to respond to desired frequencies in the microwave region. The model results show a high correlation with the experimentally observed absorption, however, several differences exist:

- The modeled peak absorption frequencies, for each resonator size, are shifted to slightly higher frequencies than observed experimentally. These shifts are slight with a minimum shift of 0.7% and maximum shift of 2.2%.
- The experimental peak absorptions are greater than the modeled peaks. Experimental absorption peaks ranged from 5 to 14 percent greater than modeled peaks.
- The modeled peak absorption decreases as resonator size decreases, while the experimental peak absorption is nearly constant for all resonator sizes. The modeled peak absorption decreased by 8 percent from the largest to smallest resonator sized metamaterial.
- The modeled absorption is symmetric about the resonant frequency while the experimental absorption is asymmetric. The experimental data, for each resonator size, show a steeper increase in absorption as the frequency increases from below the resonant frequency and a more gradual decrease in absorption as the frequency increases above the resonant frequency.
- The experimental data shows regions negative absorption by the metamaterials at frequencies below the resonant frequency.

Several possibilities exist for the variation between the model and experimental data, including inaccuracies of the physical properties of the individual materials in the model, inaccuracies in dimensions of the metamaterial structure used in the model, and inaccuracies in the experimental measurement apparatus. The values for relative permittivity and loss tangent of the dielectric, FR4, used were taken from previous numerical studies reported [50], [52]. However, those values were not consistent between different studies [50], [52]. The relative permittivity of FR4 is known to vary with manufacturer [53]. This stems from the fact that FR4 does not refer to a specific material

but a National Electrical Manufactures Association (NEMA) designated grade of a woven fiberglass reinforced epoxy laminates with specific flame resistant properties. As such, variations in physical properties occur in glass-epoxy materials designated as FR4. The relative permittivity of FR4 has also been shown to vary with frequency in the microwave region [53]. This frequency dependency was not modeled but would potential cause a shift in the peak absorption frequencies. Additionally, in the metamaterial structure manufacturing process it is unclear if an additional adhesive was used to bond the ground plane and resonators to the FR4, which would affect the relative permittivity and loss tangent values of the dielectric layer.

The conductivity of the copper resonators and ground plane were modeled with the bulk value for copper. This value was not confirmed and it is likely there is some variance from the bulk value.

The dimensions used to model the unit cell were obtained by determining the overall thickness from the ground plane to the resonator via calibers. The thickness of the resonator and the over-etched region were determined by optical profilometer measurements. The ground plane was assumed have the same thickness as the resonator (as indicated by the manufacturer) and the thickness of the dielectric layer was deduced from previous measurements $\left(overall\_thickness - 2 \times resonator\_thickness\right)$. The optical profilometer measurements necessitated the removal of resonator material. This process, particularly at these thicknesses, could have resulted in unintended removal of copper, FR4 or additional adhesives, resulting in inaccurate dimensions. The conformal infusion of epoxy resin in woven glass of FR4 material creating a non-uniform surface and the poor reflective characteristics of FR4 may have also contributed to inaccurate measurements of copper and FR4 thicknesses. Additionally, each of the optical profilometer measurements was taken once and at a single location. Average measurements from multiple locations would account for manufacturing variation and yield more reliable results. All of these combined factors may have resulted in modeling inaccuracies.

The negative absorption characteristic of the metamaterials was unexpected. This consistently occurred at values below the resonant frequency of the particular metamaterial. This indicates that at these frequencies more energy is detected at the receiving antenna from the metamaterial than from the mirror. A possible explanation for this is that the copper square resonators are acting as parasitic arrays coupled to the transmitting antenna. As such they act as passive resonators, absorbing and then re-radiating the transmitted energy out of phase, dependent on distance from the source. The phase-varying waves from multiple squares interfere with one another, modifying the radiation pattern, similar to yagi type antennas. Parasitic elements are typically one-half or one-quarter wavelength of the transmitted energy. The negative absorption was observed when the square size was less than a quarter wavelength of the incident radiation.

An additional consideration is the deviance of the estimated signal from actual signal near the endpoints of the data, which is apparent in Figure 18. This coupled with over or under filtering of the estimated signal could lead to the creation of additional fringes in the data that contribute to negative absorption values.

B. SENSOR APPLICABILITY

These metamaterial absorbers have potential to be used as part of bolometer arrays to detect spectral signatures of HPM weapons [5]. It has been demonstrated that a resistive layer with high temperature-coefficient of resistance, or bolometric layer, can be embedded in the dielectric layer of metamaterials without appreciable degradation of the absorption characteristics. As demonstrated both experimentally and numerically in this study the frequency of absorbed energy, and thus detection frequency of the microwave energy, can be controlled by the dimensions of the resonators. The sensitivity of the detector can be controlled by the thickness of the dielectric layer [5]. This dimensional tuning gives the ability to create a matrix of detectors that respond over a range of frequencies determined by resonator size, and with graded sensitivity to the detection frequencies, determined by the dielectric thickness [5]. Figure 23 illustrates an array of metamaterial absorbers with varying frequency response and sensitivity. In the rows of

the matrix the resonator sizes vary from detector to detector to corresponding to shifts in frequency response over the desired detection bandwidth, which is ideally unlimited [5]. The resonator size remains constant in the columns of the matrix corresponding to a constant frequency response; however, the thickness of the dielectric layer varies throughout the column yielding varying sensitivity to a single frequency [5]. In this type of metamaterial bolometric detector array, strong signals would result in absorption and activate a thermal response in detectors of a single frequency and several signal intensities [5]. Weak signals would generate a response in only the most sensitive detector of that frequency [5].

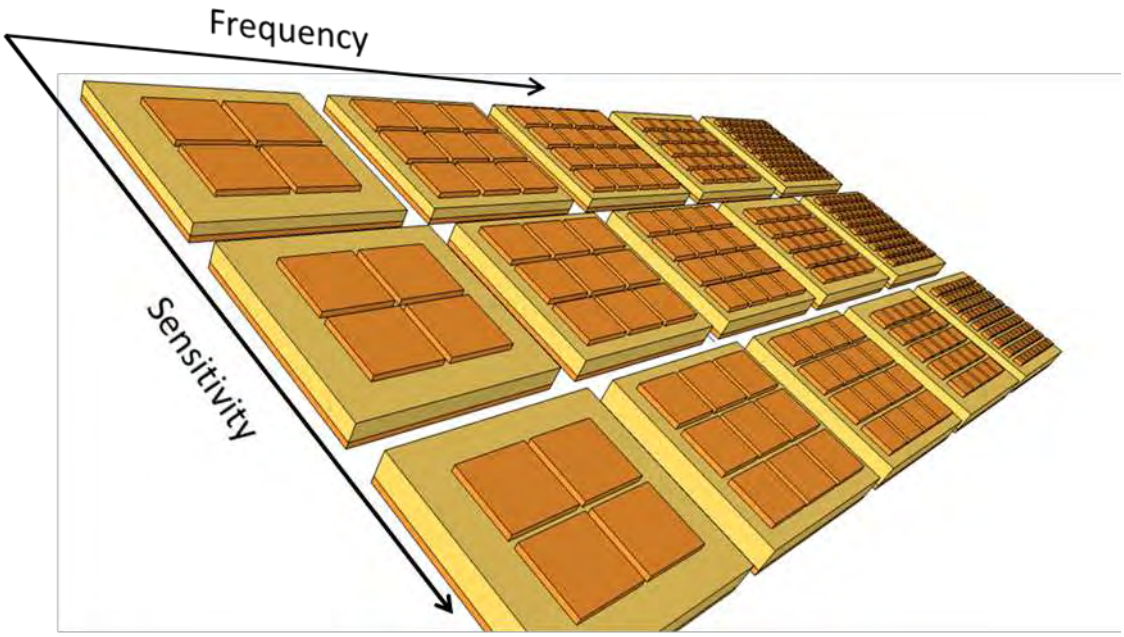

Figure 23. Metamaterial absorber array where resonator dimensions control the detection frequencies and sensitivity is controlled by the thickness of the dielectric layer, after [5].

This type of detector configuration offers several advantages:

- The need for wide-band antennas, high-gain pre-conditioning and signal processing electronics is eliminated [5].
- Bandwidth limitations are less restrictive than in current electronic microwave detection systems [5].

- This configuration is more robust than current detection systems and less susceptible to HPM attack [5].
- Fabrication processes for these types of devices is well established and would be much more cost effective than current detection systems [5].
- The response of each individual detector in this type of matrix can be stored individually in non-volatile memory elements which when properly shielded will enable the identification of the spectral signature of the HPM weapon regardless of the result of the attack [5] i.e., the spectral signature of the HPM weapon can still be obtained if even if the attack is successful, assuming the non-volatile memory can physically be recovered.
- The spectral signature of HPM weapons would provide critical information for the development of additional countermeasures.

The characteristics of the metamaterial absorbers make them ideal for this type matrix detector and spectral analysis; however, their application is not limited to this. Numerical modeling of multi-layer metamaterial structures, structures where multi-layers of dielectric and varying sized resonators stacked atop one another, has demonstrated metamaterials can also be utilized for wide-band absorption [50] in the microwave regime.

C. SPACE APPLICABILITY

The most unique and potentially most advantageous characteristic of the metamaterial detector array described above is the ability to identify the spectral signature of the HPM weapon even in the event of a successful attack. This identification is dependent on the ability to physically recover hardware from the targeted system, which is currently impractical for space applications. There are, however, several possible applications for this type of detector on spacecraft. First, this same type of detector previously described could be used on a spacecraft to detect HPM energy and transmit data prior to failure in the event of an attack. This would be particularly suited for spacecraft in constant contact with ground stations or communication relay satellites. In these instances, assuming the attack did not result in immediate failure of the satellites transmission capabilities, the spectral signature of the HPM weapon could be transmitted and at the very least there would be indications of a HPM weapon attack that would otherwise be undetected.

Another application would be to utilize the detector to trigger safe-modes aboard satellites in the event of an HPM attack. For example an imaging spacecraft, hardened against HPM energy would still be vulnerable to HPM weapon attack through back-door coupling through the optical sensor. A metamaterial microwave detector could be used to trigger an automatic self-preservation mode where the optical shutter or aperture closes and other measures are initiated such as a maneuver or rotation to avoid front-door coupling through communication antennas. In this application the detector array would likely be simpler and include only a single sensitivity for a predetermined intensity threshold over the frequency range of the detector. An additional spacecraft application for microwave metamaterial absorbers is shielding against HPM energy. Several studies have examined the basic electronic mechanisms that operate in circuits that render them susceptible to upset and damage from HPM threats [55]. Other testing focused on complete electronic platforms yield information on the susceptibility of these systems [55]. HPM radiation couples into electronics via many ingress pathways and the coupling mechanisms are not well understood [55]. Effective shielding through the absorption of HPM radiation requires an understanding of the coupling mechanisms and the electromagnetic fields in complex cavities. A recent study has resulted in a solid basis for predicting localized HPM field intensities in cavities and the HPM voltages they induce in circuits. This ability provides a foundation for designing metamaterial absorbers for generalized cavity shapes [55].

D. FUTURE WORK

In order to pursue the design of a HPM detector as described, the discrepancies in the modeled and experimental results, previously discussed, need to be resolved to reconcile the prediction of the model. The probable causes for the discrepancies, also previously discussed, may be identified through additional physical measurements of the metamaterial and the component properties, numerically through additional modeling, or through different test conditions. In particular the frequency dependence of the relative permittivity of the dielectric layer should be incorporated into the model. The negative absorption results should be investigated to determine if the cause is parasitic arrays or some other phenomenon.

When the model sufficiently predicts experimental results the frequency range for the detector as well as the power intensities should be identified through an assessment of HPM threat characteristics. With this data, the design of the metamaterial absorbers can be optimized through additional numerical modeling. With an optimized absorber design the thermal response can be simulated through the model and this data can be used to determine the bolometric layer properties for the desired sensitivities of the detector array. Once accomplished the prototype sensor array can be fabricated for experimental testing.

Of particular interest for space applications are the effects of the space environment on the materials used in the detector. This would require an assessment the orbital characteristics and intended lifetime of the detector. An assessment on corrosive effects and how that would influence the detector properties would be required to identify suitable materials for use in space.

THIS PAGE INTENTIONALLY LEFT BLANK

LIST OF REFERENCES

[1] L. Thompson and D. Gouré. *Directed-energy weapons: technologies, applications and implications*, Lexington Institute, Arlington, VA, Feb. 2003. [Online]. Available: http://lexingtoninstitute.org/wp-content/uploads/directed-energy-weapons.pdf

[2] Defense Science Board. *Report of the Defense Science Board task force on directed energy weapons and technology applications*, Office of the Under Secretary of Defense for Acquisition, Technology and Logistics, Washington, D.C., Dec. 2007.[Online]. Available: http://www.acq.osd.mil/dsb/reports/ADA476320.pdf.

[3] J. Benford, J. Swegle and E. Schamiloglu, *High power microwaves*, 2nd ed. New York: Taylor & Francis, 2007, pp. 45–49.

[4] F. Alves, D. Grbovic and G. Karunasiri, "Investigation of microelectromechanical systems bimaterial sensors with metamaterial absorbers for terahertz imaging," *Optical Eng.*, vol. 53, no. 9, pp. Sept. 2014 pp. 097103.

[5] D. Grbovic, "Metamaterial microwave microbolometer arrays for analysis of HPM radiation threats," unpublished.

[6] Electronic Warfare, JP 3–13.1, Joint Chiefs of Staff, Washington, DC, 2007, pp. I-8.

[7] B. Deveci, "Direct-energy weapons: invisible and invincible," M.S. thesis, Dept. of Info. Sc. Naval Postgraduate School, Monterey, CA, 2007.

[8] J. Benford, "Space Applications of High-Power Microwaves," in *IEEE Transactions on Plasma Science*, 2008, vol. 36, pp. 569–581..

[9] G Ni, B. Gao, and J. Lu, "Research on high power microwave weapons," in *Asia-Pacific Microwave Conference Proceedings,* 2005, vol. 2, pp. 4–7.

[10] Th. H.G.G. Weise, et al., "Overview of directed energy weapon developments," in *12th Symposium on Electromagnetic Launch Technology,* 2004, pp. 483–489.

[11] D.M. Sowders, "High power microwave and ultra wideband: a primer on high power RF," Air Force Material Command, Phillips Laboratory, Advanced Weapons and Survivability Dir., Kirtland AFB, NM, 1996.

[12] J. A. Brunderman. "High power radio frequency weapons: a potential counter to U.S. stealth and cruise missile technology," Air War College, Maxwell AFB, AL, 1999.

[13] X. Pasco, "Various threats of space systems," in *Handbook of Space Security*, K. U. Schrogl, et al., Eds., New York: Springer, 2015, pp. 663–678.

[14] Y. Tadjdeh, (Jul., 2014). New Chinese threats to U.S. space systems worry officials," *National Defense* [Online]. Available: http://www.nationaldefensemagazine.org/archive/2014/July/Pages/NewChineseThreatstoUSSpaceSystemsWorryOfficials.aspx.

[15] U. S. Senate. 113th Congress, 2nd Session 2014 (2014, Jul. 17). Department of defense authorization of appropriations for fiscal year 2015 and the future year's defense program: Testimony before the Subcommittee on Strategic Forces, Committee on Armed Services. [Online]. Available: https://www.congress.gov/congressional-report/113th-congress/senate-report/211/1.

[16] C. Wilson, "High altitude electromagnetic pulse and high power microwave devices: threat assessments." Congressional Research Service, Washington, DC, RL32544, Jul. 2008.

[17] E. M. Walling, "High power microwaves: strategic and operational implications for warfare," Air War Coll., Occasional Paper No. 11, Maxwell AFB, AL, Feb. 2000.

[18] W. Possel, "Lasers and missile defense: new concepts for space-based and ground-based laser weapons," Air War Coll., Occasional Paper No. 5, Maxwell AFB, AL, Jul. 1998.

[19] T. Cui, D. Smith and R. Liu, "Introduction to Metamaterials," in *Metamaterials*, T. Cui, D. Smith and R. Liu, Eds., New York: Springer, 2010, pp. 1–5.

[20] J. Pendry, "Metamaterials and the control of electromagnetic fields," in *Conference on coherence and quantum optics*, Rochester, NY, 2007, pp. CMB2 1–11.

[21] N. Landy, et al., "Perfect metamaterial absorber," *Phys. Rev. Lett.*, vol. 100, no. 20, pp. 207402, May 2008.

[22] J. Pendry and D. Smith, "The Quest for the Superlens," *Sci Am.*, vol. 295, no. 1, pp. 60–67, Jul. 2006.

[23] F. Alves et al., "Strong terahertz absorption using SiO2/Al based metamaterial structures," *Appl. Phys. Lett.*, vol. 100, no. 11, pp. 111104, Mar. 2012.

[24] F. Alves et al., "MEMS bi-material terahertz sensor with integrated metamaterial absorber," *Opt. Lett.*, vol. 37, no. 11, pp. 1886–1888, 2012.

[25] T. Maier and H. Bruckl, "Wavelength-tunable microbolometers with metamaterial absorbers," *Opt. Lett.*, vol. 34, no. 19, pp. 3012–3014, Oct. 2009.

[26] L. Huang and H. Chen, "Multi-band and polarization insensitive metamaterial absorber," *PIER*, vol. 113, pp. 103–110, Jan. 2011.

[27] X. Shen et al., "Polarization-independent wide-angle triple-band metamaterial absorber," *Opt. Expr.*, vol. 19, no. 10, pp. 9401, May 2011.

[28] H. Li et al., "Ultrathin multiband gigahertz metamaterial absorbers," *J. Appl. Phys.*, vol. 110, no. 1, pp. 014909, Jul. 2011.

[29] Q.Y.Wen et al., "Dual band terahertz metamaterial absorber: design, fabrication, and characterization," *Appl. Phys. Lett.*, vol. 95, no. 24, pp. 241111, Dec. 2009.

[30] L. Huang et al., "Experimental demonstration of terahertz metamaterial absorbers with a broad and flat absorption band," *Opt. Lett.*, vol. 37, no. 2, pp. 154– 156, Jan. 2012.

[31] H. Tao et al., "A dual band terahertz metamaterial absorber," *J. Phys. D: Appl. Phys.*, vol. 43, no. 22, pp. 225102, Jun. 2010.

[32] X. J. He et al., "Dual-band terahertz metamaterial absorber with polarization insensitivity and wide incident angle," *PIER*, vol. 115, pp. 381–397, Apr. 2011.

[33] Y. Ma et al., "A terahertz polarization insensitive dual band metamaterial absorber," *Opt. Lett.*, vol. 36, no. 6, pp. 945–947, Mar. 2011.

[34] B. Zhang et al., "Polarization-independent dual-band infrared perfect absorber based on a metal-dielectric-metal elliptical nanodisk array," *Opt. Expr.*, vol. 19, no. 16, pp. 15221, Aug. 2011.

[35] X. Liu et al., "Taming the blackbody with infrared metamaterials as selective thermal emitters," *Phys. Rev. Lett.*, vol. 107, no. 4, pp. 045901, Jul. 2011.

[36] J. Hao et al., "Nearly total absorption of light and heat generation by plasmonic metamaterials," *Phys. Rev. B*, vol. 83, no. 16, pp. 165107, Apr. 2011.

[37] H. Atwater, "The promise of plasmonics," *Sci Am*, vol. 296, no. 4, pp. 56–62, Apr. 2007.

[38] Y. Liu and K. Yao, "Plasmonic metamaterials," *Nanotechnology Rev.,* vol. 2, no. 2, pp. 177–210, Jan. 2013.

[39] B. T. Kearney, "Enhancing microbolometer performance at terahertz frequencies with metamaterial absorbers," Ph.D. dissertation, Phy. Dept., Naval Postgraduate School, Monterey, CA, 2013.

[40] H. Nornikman et al., “Effect of single complimentary split ring resonator structure on microstrip patch antenna design,” in *2012 IEEE Symposium on Wireless Technology and Applications*, Bandung, Indonesia 2012, pp. 239–244.

[41] Martın, F., J. Bonache, F. al Falcone, M. Sorolla, and R. Marques. “Split ring resonator-based left-handed coplanar waveguide.” *Appl. Phys. Lett.,* vol. 83, no. 22, pp 4652–4654, Dec. 2003.

[41] S. Das, et al., “Novel compact CPW filter for MICs using metamaterial structures,” *in IEEE Mediterranean Microwave Symposium*, 2011, pp. 286–289.

[43] D. J. Kern, et al., “The design synthesis of multiband artificial magnetic conductors using high impedance frequency selective surfaces,” *in IEEE Transactions on Antennas and Propagation*, 2005, vol. 53, pp. 8 -17.

[44] Y. L. Loo, et al., “Broadband microwave Luneburg lens made of gradient index metamaterials,” *J. Opt. Soc. Am. A*, vol. 29, no. 4, pp 426–430, Apr. 2012.

[45] F. Alves et al., “Strong terahertz absorption using SiO2/Al based metamaterial structures,” *Appl. Phys. Lett.*, vol. 100, no. 11, pp. 111104, Mar. 2012.

[46] T. Maier and H. Bruckl, “Wavelength-tunable microbolometers with metamaterial absorbers,” *Opt. Lett.*, vol. 34, no. 19, pp. 3012–3014, Oct. 2009.

[47] Y. Todorov et al., “Optical properties of metal-dielectric-metal microcavities in the THz frequency range,” *Opt. Expr.*, vol. 18, no. 13, pp. 13886, Jun. 2010.

[48] H. T. Chen, “Interference theory of metamaterial perfect absorbers,” *Opt. Expr.*, vol. 20, no. 7, pp. 7165–7172, Mar. 2012.

[49] Q.-Y Wen et al., “Transmission line model and fields analysis of metamaterial absorber in the terahertz band,” *Opt. Expr.*, vol. 17, no. 22, pp. 20256–20265, Oct. 2009.

[50] H. Luo, X. Hu, Y. Qiu and P. Zhou, “Design of a wide-band nearly perfect absorber based on multi-resonance with square patch,” *Solid State Communications*, vol. 188, pp. 5–11, Jun. 2014.

[51] “Perfectly Matched Layers (PMLs),” COMSOL 4.3 Help Documentation. http://www.comsol.com/support/helpdoc/

[52] W. Zhu and X. Zhao, “Metamaterial absorber with dendritic cells at infrared frequencies,” *J. Opt. Soc. Am.*, vol. 26, no. 12 pp. 2382–2385, Dec. 2009.

[53] J.R. Aquilar, et al., “The microwave and RF characteristics of FR4 substrates,” in *IEE Colloquium on Low Cost Antenna Technology*, London, 1998, pp. 2/1-2/6.

[54] D. Grbovic and G. Karunasiri. (2009, Apr. 30) Fabrication of Bi-material MEMS detector arrays for THz imaging," SPIE Proc. [Online]. 7311(08). Available: http://proceedings.spiedigitallibrary.org/proceeding.aspx?articleid= 777364

[55] J. Rodgers. (2012, Mar.). *Protection of electronic systems from the effects of high-power microwave (HPM) and ultra-wideband (UWB) sources*, Univ.of Maryland, Inst. for Res. in Elect. and Ap. Phy. College Park, MD. [Online]. Available: http://oai.dtic.mil/oai/oai?verb=getRecord&metadataPrefix=html &identifier=ADA567604

THIS PAGE INTENTIONALLY LEFT BLANK

INITIAL DISTRIBUTION LIST

1. Defense Technical Information Center
   Ft. Belvoir, Virginia

2. Dudley Knox Library
   Naval Postgraduate School
   Monterey, California